Developmental Biology 364 (2012) 162–177

Contents lists available at SciVerse ScienceDirect

Developmental Biology

journal homepage: www.elsevier.com/developmentalbiology

Matrix metalloproteinase 9/gelatinase B is required for neural crest cell migration

Efrat Monsonego-Ornan [a], Jenia Kosonovsky [a,b,1], Avi Bar [a,b,1], Lee Roth [a,b], Veatriki Fraggi-Rankis [a,b], Stav Simsa [a], Ayelet Kohl [b], Dalit Sela-Donenfeld [b,*]

[a] The Institute of Biochemistry and Nutrition, The Robert H. Smith Faculty of Agriculture, Food and Environment, The Hebrew University, Rehovot, Israel
[b] Koret School of Veterinary Medicine, The Robert H. Smith Faculty of Agriculture, Food and Environment, The Hebrew University, Rehovot, Israel

ARTICLE INFO

Article history:
Received for publication 25 May 2011
Revised 30 January 2012
Accepted 31 January 2012
Available online 8 February 2012

Keywords:
Epithelial-to-mesenchymal transition
Neural tube
Cell migration
Delamination
ECM
MMP

ABSTRACT

This study determined the role of MMP9/gelatinase B during the migration onset of Neural Crest Cells (NCC) in avian embryos. NCC are neuroepithelial progenitors that convert into mesenchyme and migrate along defined paths throughout the embryo. To engage in migration, NCC loose cell contacts, detach from the neural tube and invade the surrounding environment. Multiple signals and transcription factors that regulate these events have been identified. Nevertheless, little is known regarding effectors that act downstream to execute the actual NCC migration. Matrix metalloproteinases (MMPs) compose a large family of enzymes whose principal substrates are basement membranes, adhesion proteins and the extracellular matrix (ECM) components. A major subgroup of MMPs, the gelatinases (MMP9 and 2) are central to many adult physiological and pathological processes, such as tumor metastasis and angiogenesis, in which cell–cell and cell–matrix contacts are degraded to allow migration. As NCC undergo similar processes during development, we hypothesized that MMP9 may also promote the migration of NCC.

MMP9 was found to be expressed in delaminating and migrating NCC of both cranial and trunk axial levels. Blocking MMP9 resulted in a dramatic inhibition of NCC delamination and migration, without perturbing specification or survival. This inhibition occurred at regions containing both premigratory and migrating cells, indicative for the central role of MMP9 in executing the detachment of NCC from the neural tube as well as their migration. Conversely, excess MMP9 enhanced mesenchymalization and delamination of NCC and accelerated progenitors to undergo precocious migration. Examination of the mechanistic activity of MMP9 revealed its capability to degrade the adhesion molecule N-cadherin as well as the basement-membrane protein laminin within or around NCC, respectively. Altogether, our study reveals MMP9 as a novel effector which is required for NCC delamination and migration.

Introduction

Neural crest cells (NCC) are a discrete cell-population that arises from the dorsal neural tube and migrate along defined pathways throughout the embryo. NCC give rise to a variety of derivatives including sensory neurons/ganglia, Schwann cells, pigments and endocrine cells, as well as generate most of the craniofacial cartilage and bones (for reviews see Barembaum and Bronner-Fraser, 2005; Erickson and Reedy, 1998; Kalcheim and Burstyn-Cohen, 2005; Le-Douarin and Kalcheim, 1999). Prior to their migration, NCC constitute an integral part of the neural tube, whereas subsequently, they undergo epithelial-to-mesenchymal transition (EMT) and detach from the neuroepithelium as mesenchymal cells (reviewed in Le-Douarin and Kalcheim, 1999; Raible, 2006; Taylor and LaBonne, 2007). This dramatic process requires changes in cellular and extra-cellular behaviors such as the breakdown of the basal lamina around the dorsal neural tube, switches in expression of cell–cell and cell–matrix adhesion molecules, modification in cytoskeleton assembly, development of motility and appearance of guidance cues (Barembaum and Bronner-Fraser, 2005; Gammill and Roffers-Agarwal, 2010; Kulesa and Gammill, 2010; Le-Douarin and Kalcheim, 1999; Trainor, 2005).

A central signal that coordinates the onset of NCC migration is the bone morphogenetic protein (BMP). An interplay between BMP4 and its inhibitor noggin in the dorsal neural tube determines the levels of BMP signals required for NCC delamination by stimulating Wnt signaling and N-cadherin cleavage (Burstyn-Cohen and Kalcheim, 2002; Burstyn-Cohen et al., 2004; Sela-Donenfeld and Kalcheim, 1999, 2000, 2002; Shoval et al., 2007). Recently, gradients of mesodermal retinoic acid and FGF were also found to regulate the timing of NCC migration by modulating the activity of Wnt, BMP and noggin (Martinez-Morales et al., 2011). A complex network of DNA binding proteins, such as Sox8–10, Snail and Foxd3, also orchestrates NCC delamination intrinsically (Basch and Bronner-Fraser, 2006; Cano et al., 2000; Cheung et al., 2005; Gammill and Bronner-Fraser, 2003; Trainor, 2005). In addition, modulations in adhesion molecules, ADAM proteases and small GTPases are also essential for this process (Alfandari et

* Corresponding author. Fax: +972 8 9467940.
E-mail address: seladon@agri.huji.ac.il (D. Sela-Donenfeld).
[1] These two authors contributed equally to the work.

0012-1606/$ – see front matter © 2012 Elsevier Inc. All rights reserved.
doi:10.1016/j.ydbio.2012.01.028

al., 1997; Coles et al., 2007; Cousin et al., 2011; Erickson, 1986; Groysman et al., 2008; Jhingory et al., 2010; Nakagawa and Takeichi, 1998; Newgreen and Minichiello, 1995; Shoval et al., 2007; Wei et al., 2010). Yet, soluble effectors that should act downstream to these pathways to execute the actual detachment and migration of NCC by modifying cell–cell and cell–matrix interactions, are much less known (Erickson and Reedy, 1998; Kalcheim, 2000; Radisky, 2005; Taylor and LaBonne, 2007; Thiery et al., 1988).

Proteolysis is a major process leading to dramatic changes in cell migration and contacts by affecting cell–cell/cell–extracellular matrix (ECM) adherence, ECM and basement membrane degradation, releasing of bioactive fragments, sequestering of growth factors and shedding of cell-surface proteins (Mott and Werb, 2004). The matrix metalloproteinases (MMPs) are a large family of secreted enzymes able to degrade structural proteins of the ECM and basal lamina in different physiological and pathological contexts (Hasky-Negev et al., 2008; Nelson et al., 2000; Sternlicht and Werb, 2001). 25 members have been identified in vertebrates (Lohi et al., 2001; Nagase and Woessner, 1999) and grouped into 4 main subfamilies, according to their structure and substrate specificity; collagenases, gelatinases, stromelysins and the membrane-type MMPs. Each of these has a distinct, but often overlapping, substrate specificity that together can cleave numerous substrates, including virtually all ECM proteins (Sternlicht and Werb, 2001). Several MMPs were also shown to digest cadherins and integrins, leading also to changes in cell–cell and cell–ECM adherence. Moreover, some MMPs were found to activate others by cleaving their pro-domains (Sternlicht and Werb, 2001), resulting in a hierocracy of events that regulate MMPs' activation and function. Based on these activities, these proteases play a key role in EMT and cell migration in angiogenesis, metastasis and tissue remodeling (Coussens and Werb, 2002; McCawley and Matrisian, 2000; Reich et al., 2005; Visse and Nagase, 2003).

The gelatinase subgroup of MMPs, composed solely of MMP2 and MMP9, can hydrolyze denatured collagens (gelatins) with very high efficiency, as well as native collagen types I, IV, fibronectin and laminin (Morrison et al., 2009; Rodriguez et al., 2010; Vu and Werb, 2000). MMP9 was previously found to be involved in mammalian bone formation by promoting vascular invasion into the growth plate (Vu et al., 1998). Although its molecular mode of action in tissue invasion is not certain, it is speculated that MMP9 may release growth factors from the matrix (Engsig et al., 2000; Sternlicht and Werb, 2001) as well as contribute to degradation of the ECM. Notably, the avian MMP9 possesses a number of biochemical and amino acid sequence features that differs it from its mammalian counterpart; it has low sequence similarity to the mammalian enzyme (59% on the protein level), lacks the type V collagen domain and can cleave fibronectin, which is not a substrate for mammalian MMP9 in in vitro assays (Hahn-Dantona et al., 2000). We have previously studied the expression and role of avian MMP9 in the process of growth plate vascularization during endochondral ossification in the chicken, confirming this protein to be indeed the avian homologue of the mammalian MMP9 (Dan et al., 2009; Hasky-Negev et al., 2008; Leach and Monsonego-Ornan, 2007; Simsa et al., 2007a; Tong et al., 2003).

As NCC undergo EMT and acquire motility, it is highly possible that MMPs play roles in this unique cell population. To date, only very few studies examined these proteases in NCC; MMP2 was demonstrated to be transiently expressed in avian NCC, and its inhibition perturbed some (but not all) phases of NCC migration (Duong and Erickson, 2004). MMP2 and the general MMP inhibitor TIMP2 were also suggested to be involved at later stages, during migration of NCC toward the heart and gut (Anderson, 2010; Cai et al., 2000; Cantemir et al., 2004). Descriptive data further demonstrated *MMP14* expression in NCC of *Xenopus laevis* embryos, (Harrison et al., 2004; Tomlinson et al., 2009), and *MMP8* in mouse NCC (Giambernardi et al., 2001).

This study analyzed whether other, yet unidentified MMPs, are implicated in NCC migration, and discovered that MMP9/gelatinase B is expressed in avian NCC during their emigration and migration at the trunk and cranial levels of the neural axis. Detailed gain-and-loss-of-function experiments revealed that MMP9 is essential to execute NCC EMT and migration, and that this activity is mediated by degradation of laminin and N-cadherin. Together, this study uncovers a novel role for MMP9 in promoting delamination and migration of early embryonic NCC cells.

Materials and methods

Embryos

Fertile Lohman chick eggs were incubated at 38 °C. For in vivo procedures, eggs were windowed and embryos visualized by injecting black ink below the blastodisc. Following manipulations, embryos were incubated up to the required stages, fixed in 4% paraformaldehyde (PFA), dehydrated in 100% methanol, and stored at −20 °C.

MMP9 cloning, transfection and zymography assay

Chick MMP9 (cMMP9) expression construct was generated by cloning a 1349 bp fragment from avian chondrocyte cDNA (Tong et al., 2003) containing an ATG start codon, signal peptide, prodomain sequence, active site, fibronectin II repeat domain and zinc binding sequence. Primers used were: forward- ATGCTCCTGGCCCCGCT and reverse- GGCTCAGGGCCAGAGCC. PCR amplification was performed in 1 unit Isis™ DNA polymerase using the following program: 95 °C/5 min and 30 cycles of 95 °C/35 s, 53 °C/45 s, 72 °C/45 s. Fragment was inserted into pCDNA3 plasmid (Invitrogen, New Mexico, USA) in EcoRV sites. Mouse MMP9 (mMMP9) expression construct was generated by cloning a 2193 bp fragment from mMMP9 cDNA-containing vector 6309245 (Thermo Fisher Scientific Co., USA), containing an ATG start codon, signal peptide, prodomain sequence, active site, fibronectin II repeat domains, zinc binding sequence and hemopexin domain. Primes used were: forward- GCGATATCCACCATGAGTCCCTGGCAGC, and reverse-GAGAGCTCCAGCTAGCACCTTTCCCTCG. PCR amplification was performed in 1 unit Isis™ DNA polymerase using the following program: 95 °C/5 min and 35 cycles of 95 °C/30 s, 65 °C/30 s, 72 °C/3 min. Fragment was inserted into pCAGGS-IRES-GFP vector in EcoRV (forward) and SacI (reverse) sites.

Transfection of 10 μg cMMP9 cDNA was performed in rat chondrosarcoma (RCS) cell line as previously described (Ben-Zvi et al., 2006). Selection of stably-transfected cells was obtained by addition of 1 μg/ml G418 (Monsonego-Ornan et al., 2000). For zymography assay, cells or media samples were separated on a gelatin-impregnated gel under non-reducing conditions to test MMP9 gelatinolytic activity (Dan et al., 2009). Gels were washed in 2.5% Triton X-100, incubated at 37 °C/16 h in calcium assay buffer, and stained with 0.5% Coomassie R-250 (Simsa et al., 2007b).

RT-PCR from embryos and neural tube explants

Total RNA was purified from whole embryos of 10, 16 and 25 somites, or from pools of isolated mesoderm or neural tubes, collected from similar stages. RNA was also collected from isolated neural tube explants, either before or after culturing them in ex-vivo conditions, as well as from NCC that migrated away from the cultured neural tubes. Reverse transcription (RT) was performed using the RT-for-PCR Kit (Clontech, CA, USA). cDNA was amplified by PCR in 25 μl reaction solution containing 2 μl cDNA, 1 unit Taq-polymerase, 25 μM of each dNTP and 2 μM primers. Primers used were: MMP9 forward- ACCGTGCC GTGATAGATGAT and reverse- AGCCACCAAGAAGATGCTGT. PCR was carried out using the following program: 95 °C/5 min followed by 35 cycles of 94 °C/40 s, 56 °C/45 s and 72 °C/45 s.

Explants of neural tubes

Trunk region of embryos of 16–18 somites were sectioned at the level of the anterior segmental plate plus the last 3 somite pairs. The cranial region of 6–8 somite-old embryos was sectioned at the hindbrain level. Neural primordia, consisting of neural tube with pre-migratory NCC, were isolated from the adjacent tissues using 25% pancreatin and explanted onto dishes pre-coated with 50 μg/ml fibronectin (Sela-Donenfeld and Kalcheim, 1999). Neural tube explants were incubated with the following media: (i) conditioned media from control RCS cells, (ii) conditioned media from MMP9-producing RCS cells, (iii) control CHO-S-SFM II media (Gibco BRL, MD, USA) containing 1% or 2.5% DMSO, (iv) CHO-S-SFM II media containing 5 μM or 12.5 μM MMP9 inhibitor I (Calbiochem, CA, USA), dissolved in 1% or 2.5% DMSO, respectively, (v) control or 12.5 μM MMP9 inhibitor I-containing media (as above) supplemented with Hoechst stain (40 μg/ml, Sigma MO, USA). In rescue experiments, explant media, consisting of control or 12.5 μM MMP9 inhibitor I, were added for overnight after which media were replaced with fresh control media. In some experiments, a layer of control or MMP9-producing RCS cells was prepared, on top of which explants were placed. Unless indicated otherwise, explants were grown for 16 h, fixed in 4% PFA or 100% methanol and preceded for immunostaining or microscopy visualizations. In some other experiments, explants were incubated in control CHO-S-SFM II + Hoechst for 5 h followed by addition of 12.5 μM MMP9 inhibitor I in 2.5% DMSO or 2.5% DMSO as control for overnight.

In ovo procedures

Cell grafting

Control or MMP9-secreting RCS cells were grown to confluence, pelleted and re-suspended in minimal volume of DMEM medium (Sela-Donenfeld and Kalcheim, 1999). The vitelline membrane of embryos of 14–18 somites was removed at the level corresponding to the segmental plate and a slit was performed along the dorsal edge of the neural tube. Injection of cells was performed on top of the neural tube using a pulled glass capillary. Embryos were developed for further 16 h before fixation.

Addition of MMP9

Conditioned media from control or MMP9 cells were injected into the lumen of the cranial and cervical neural tubes in embryos of 8–9 somites. Injection was performed twice in 3 h intervals. Embryos were fixed 3 h after the second injection.

Inhibition of MMP9

MMP9 inhibitor I (125 μM in 25% DMSO, dissolved in DMEM media), or control solution (25% DMSO in DMEM) were injected twice at 4 h intervals into the lumen of the caudal neural tube of 16 somite-embryos or into the cranial neural tube of 6-to 8-somite-embryos, using pulled glass capillary. Embryos were incubated for 16 h before fixation. For CM-DiI injections, CM-DiI (C-7000, Molecular Probes) was dissolved in 100% ethanol to a concentration of 1 mg/ml. Prior to injection, it was further diluted to a final concentration of 0.1 mg/ml in 125 μM MMP9 inhibitor I solution in 10% sucrose. Solution was injected at the caudal neural tube of 12-somite embryos.

Electroporation

FITC-conjugated MMP9 morpholino (MO) antisense oligonucleotides, directed against exon2–intron2 junction, or control MO sequence (GeneTools, OR, USA), were diluted in PBS to a working concentration of 2 mM. pCAGGS-IRES-GFP vector over expressing MMP9 or empty IRES-GFP vector were diluted in 1.25 M NaCl, 50 mM Tris–Cl, pH 8.5 to a concentration of 5 μg/μl. MOs and plasmids were injected into the neural tube of embryos at similar stages/axial levels as described above using pulled glass capillary. Electrodes were placed at the left and right sides of the embryo. Electroporation was performed with a BTX 3000 electroporator using four 45 ms pulses of 16 V with 300 ms pulse intervals (Itasaki et al., 1999; Sela-Donenfeld et al., 2009; Weisinger et al., 2008). Embryos were incubated for 16 h before fixation. The MO sequences are: MMP9: 5′-GTACCCATCACCTGCTCTTGGCTG3′ and Control 5′-CCTCTTACCT-CAGTTACAATTTATA-3′. For rescue experiments, MO-electroporated embryos were let to develop for 6 h before injection of MMP9-media into the neural tube. Lumen embryos were incubated for additional 10 h before fixation.

In situ hybridization (ISH) and immunohistochemistry/immunofluorescence (IHC, IFC)

In situ hybridization (ISH) on whole-mounted embryos or on paraffin-sections was performed as described before (Sela-Donenfeld and Kalcheim, 1999), using DIG or fluorescein-labeled probes against chick *MMP9* (Tong et al., 2003), *Foxd3* (Groysman et al., 2008), Krox20 (Weisinger et al., 2008) and Cad6B (Sela-Donenfeld and Kalcheim, 1999), detected by alkaline phosphatase (AP)-coupled anti-DIG or anti-fluorescein antibodies and NBT/BCIP or Fast-red substrates (Roche, Basel, Switzerland). Immunostaining on whole-mounted embryos, neural tube explants, as well as on paraffin or frozen sections was performed by blocking the samples with 3% BSA/PBS and incubation with the following antibodies; mouse-anti HNK1 (1:500, BD Pharmingen, CA, USA), mouse anti N-cadherin (extracellular domain) (1:400, Sigma MO, USA), rabbit-anti laminin (1:100, Sigma MO, USA), rabbit-anti phospohystone 3 (1:50, Santa Cruz Biotechnology, CA, USA), or rabbit anti-MMP9 (1:100, Abcam, CA, USA) at 4 °C/16 h. Antigen retrieval was performed prior to addition of laminin and N-cadherin antibodies to sections by boiling the sections for 5 min in 100 mM Tris pH 9.5. Secondary anti-mouse Alexa 488, anti-rabbit Alexa 488, anti-rabbit Alexa 594 and anti-mouse Alexa 594 (all 1:500, Molecular Probes, CA, USA), or anti-mouse HRP (1:300, Sigma MO, USA) antibodies were added at RT for 2 h after which embryos were visualized under fluorescence microscopy or stained with ACE substrate system (LabVision, CA, USA) to reveal HRP activity. To detect FITC-conjugated-MO oligonucleotides, AP-coupled anti-fluorescein antibody (1:2000, Roche, Basel, Switzerland) was added for 16 h at 4 °C, followed by addition of NBT/BCIP substrate. Actin filaments were stained by incubating explants with Phalloidin (1:500 Sigma MO, USA) for 1 h at RT followed by washes with PBS/Tween. Cell nuclei were visualized with 4′,6′-diamidino-2-phenylindole (DAPI) (1:7500, Vector Laboratories, CA, USA) for 20 min at RT.

Data analysis and imaging

Quantification of migratory NCC in explants was calculated as a mean of 5–10 explants per treatment, out of 20–25 embryos showing a similar phenotype. The area occupied by migrating NCC was calculated by ImageJ software for area-measurements using the following formula: total area occupied by both 'epithelioid' NCC plus all mesenchymal NCC, divided by the total area of the neural tube. Area of mesenchymal cells was determined by calculating the average area of 10 separated $HNK1^+$ cells and thereafter multiplying it by the number of mesenchymal cells. In timed-inhibition experiments, the migration areas of NCC after overnight experiment were calculated as described above, with subtraction of the migratory NCC areas after the first 5 h. In all experiments bars represent mean areas of the results in arbitrary units and standard deviation is provided. Significance of results was determined using the unpaired Student's *t*-test. Quantification of migratory NCC in CM-DiI experiments was performed by counting DiI + HNK1 positive cells in both sides of the neural tube in 5

subsequent sections of 3 independent embryos. Results represent mean of number of cells.

Summary of total embryos and percentages for each experiment and treatment are provided in Table 1.

Whole embryos were analyzed under SZX17 stereomicroscope (Olympus). Explants and sections were analyzed using Eclipse E400 upright microscope (Nikon) or SZX17 stereomicroscope (Olympus). All Images were taken with DP70 CCD camera (Olympus) and DP controller software.

Results

MMP9 is expressed in pre-migrating and migrating NCC

The gelatinase subfamily of MMPs is composed of two members, MMP9 and MMP2 (Hahn-Dantona et al., 2000; Malemud, 2006a). As MMP2 was previously suggested to be involved in NCC migration (Cai et al., 2000; Cantemir et al., 2004; Duong and Erickson, 2004), we were set to determine whether the other gelatinase, MMP9, plays a role in NCC migration. We first examined its expression in various embryonic stages and axial levels where NCC migration occurs, using RT-PCR (Fig. 1A). RNA was extracted from pools of whole embryos of 10, 15, 25 somites, stages when NCC migrate from cranial, vagal and trunk levels of the neural axis respectively, and from isolated neural tubes or paraxial mesoderm to examine whether MMP9 is expressed at areas associated with NCC delamination and migration. *MMP9* was found in all examined stages as well as in the purified mesoderm and neural tubes. In addition, *MMP9* mRNA was expressed in ex-vivo explants obtained from hindbrain levels of 5–8 somite-stage embryos, before or after culturing the neural tube, as well as in NCC that detached from the explants and migrated in the dish (Fig. 1A′). Together, these results indicated the presence of MMP9 transcripts in NCC as well as in regions where cells migrate into.

To further characterize the spatial distribution of *MMP9*, ISH was performed on whole-mounted embryos and on transverse sections, using MMP9-specific antisense probe (Figs. 1B,C,E,G,H,I). *MMP9* expression was compared with expression of other genes such as *Cad6B* and *Foxd3* (Figs. 1D,F,G) which mark premigratory and migrating NCC (Dottori et al., 2001; Nakagawa and Takeichi, 1995) as well as with *Krox20* (Fig. 1C), which served to label the odd-numbered rhombomeres of the hindbrain (Nieto et al., 1991). *MMP9* is expressed in the dorsal part of the cranial neural tube in embryos of 15 somites, as well as in the migratory routes of NCC into the mid-and hindbrain mesoderms (Figs. 1B,C,H). Co-labeling of *MMP9* and *Krox20* (Fig. 1C) further demonstrates the localized *MMP9* expression in the typical streams of NCC adjacent to the even-numbered segments, which are *Krox20*-negative (Farlie et al., 1999; Graham and Lumsden, 1996). Further confirmation for the specific *MMP9*-expression in the migrating hindbrain NCC is evident by its similar distribution to that of *FoxD3* (Fig. 1D). At the trunk level of embryos of 25 somites, *MMP9* is shown in the dorsal neural tube, in NCC during their migration toward the paraxial mesoderm and at the anterior half of somites (Figs. 1E,G,I). The co-localization of MMP9 and Cad6B at the dorsal tube (E–G) further confirms the specific MMP9-expression in pre-migratory trunk NCC. This analysis, together with our RT-PCR results, indicates that *MMP9* mRNA is distributed in the cranial and trunk NCC during their detachment from the neural tube and their migration.

To confirm the presence of MMP9 protein in NCC, we next examined embryos using MMP9 antibody. Sections were taken from hindbrain (Figs. 1J–L) and trunk axial levels (Figs. 1M–O) of 15 or 25 somite-old embryos, respectively. At both stages, MMP9 was clearly evident in the emigrating and migrating NCC (Figs. 1J,L,L′,M,O,O′), as shown by co-staining with the migratory NCC marker HNK1 (Figs. 1K–L′,N–O′), validating further the identity of the MMP9-expressing cells as NCC. Notably, early-migrating NCC that were still adjacent to the neural tube seemed to express MMP9 but not HNK1 (Figs. 1L,O). This is in agreement with previous reports in which HNK1 staining in evident in NCC that are more advanced in migration (Erickson, 1988; Sela-Donenfeld and Kalcheim, 1999). The secreted MMP9 is mostly bound to NCC membrane or trapped in the ECM/basement membrane around the cells. MMP9 is also evident in ectoderm cells and in the basement membrane around the neural tube, notochord and myotome (Figs. 1J,M), as also observed by the ISH analysis (Figs. 1H,I). These regions, which are along the migratory routes of NCC, suggest that MMP9 is produced in more cells than only in NCC, implicating that, in addition to NCC themselves, their surrounding environment also produces MMP9.

Next, MMP9 distribution was examined in NCC growing in ex-vivo conditions. Explants of neural primordia that contain pre-migratory NCC were dissected from hindbrain levels of embryos of 5–8 somites, freed from accompanying tissues, and cultured in fibronectin-coated dishes. After 16 h of incubation migratory NCC were evident around the neural tube explants (Fig. 1P). Staining with MMP9 antibody revealed many migrating NCC that express MMP9 protein in the cytoplasm (Figs. 1Q,S,T). Comparison with HNK1 staining revealed more cells expressing MMP9 than HNK1 (Figs. 1R,S), probably since MMP9 expression is evident in NCC prior to HNK1, as also seen in-vivo (Figs. 1L,O, see also Newgreen and Minichiello, 1995) Alternatively, it is possible that not all NCC are HNK1-positive in the ex-vivo conditions. Some MMP9 staining was also evident in-between cells (Fig. 1T), reflecting secreted MMP9 from the NCC to the ECM. Altogether, these analyses demonstrate the expression of MMP9 mRNA and protein in the emigrating and migrating NCC, as well as in regions along their migration pathways.

Table 1
Summary of embryos examined for NCC migration following in vivo addition or inhibition of MMP9.

Treatment	Normal NCC migration	Reduced NCC migration	Enhanced NCC migration	Total percentage of altered migration
DMSO	39	4	0	9% n = 43
MMP9 inhibitor I 12.5 μM	9	39	0	81% n = 48
Control-MO	30	5	0	14% n = 35
MMP9-MO	8	29	0	78% n = 37
MMP9-MO Rescue	2	0	5	71% n = 7
Control RCS cells	12	0	0	0% n = 12
MMP9-secreting RCS cells	1	0	11	92% n = 12
Control media	9	1	0	10% n = 10
MMP9 media	3	0	8	73% n = 11
Control- empty pCAGGS	8	0	0	0% n = 8
pCAGGS mMMP9	0	0	7	100% n = 7

Data shows the number of embryos that exhibit normal, reduced or enhanced NCC migration, evaluated by HNK1 staining, and the total percentage of altered migration upon different treatments. n = total number of embryos per treatment.

Inhibition of MMP9 prevents NCC delamination and migration

To determine whether MMP9 plays a role during NCC detachment from the neural tube, we examined the effect of blocking MMP9 activity on NCC emigration in ex-vivo explants, using a pharmacological inhibitor (Fig. 2). Explants of neural primordia were dissected from either the segmental plate plus 3 posterior somites of embryos of 16–18 somites (Figs. 2A–F), or from hindbrain levels of embryos of 6–8 somites (Figs. 2G–L). These regions contain predominantly specified NCC, prior to their onset of migration (Sela-Donenfeld and Kalcheim, 1999). A specific MMP9 inhibitor, MMP9 inhibitor I (Levin et al., 2001) was added to the explants media in two different concentrations — 5 μM or 12.5 μM. Control explants were treated with DMSO in equivalent amounts to those used to dissolve the inhibitor (1% or 2.5% DMSO, respectively). In general, after 16 h of incubation, NCC largely failed to

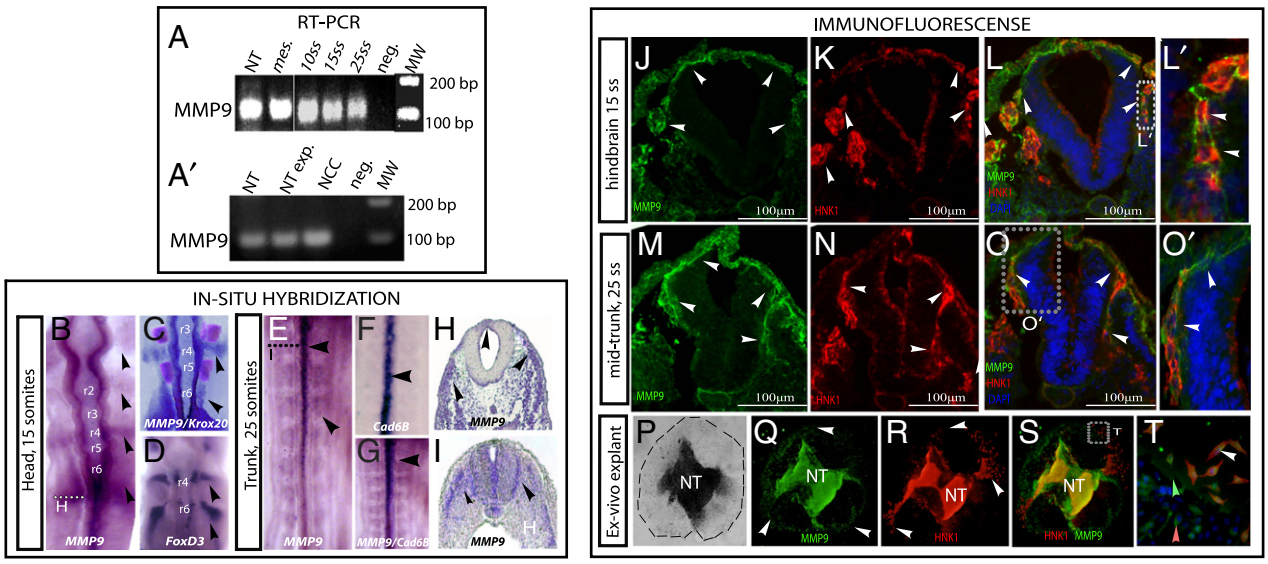

Fig. 1. MMP9 is expressed in NCC. (A): RT-PCR analysis on mRNAs purified from whole embryos of 10, 15, 25 somites or from pools of isolated neural tubes/paraxial mesoderm obtained from similar stages. (A′): RT-PCR analysis on mRNAs purified from neural-tube explants obtained from hindbrain levels of 5–8 somite-old embryos, either before or after culturing them in ex-vivo conditions, as well as from NCC that migrated away from the explants. Primer pairs used in (A,A′) were directed against a 120 bp long sequence of chick MMP9. (B–G): In situ hybridization on whole-mounted embryos of 15/25 somites labeled with RNA probe against MMP9 (B,C,E,G), Krox20 (C), FoxD3 (D) and Cad6B (F,G). Embryo in (C) was double-labeled with MMP9 (blue) and Krox20 (purple) probes. Image in (G) is a digital merge of two identical embryos (E,F) stained with MMP9 (E) and Cad6B (F). (H,I): serial sections taken from the dotted areas in B,E. Black arrowheads in (B–I) indicate NCC which express MMP9 (B,C,E,G,H,I), FoxD3 (D), or Cad6B (F,G). (J–O): Immunolabeling of transverse sections obtained from embryos of 15/25 somites using MMP9 (green,J,L,M,O) or HNK1 (red, K,L,N,O) antibodies. Blue staining in (L,O) represents DAPI staining. White arrowheads indicate MMP9 or HNK1 positive cells. Panels L′,O′ are enlargement of the boxed areas in panels L,O. (P–T): immunolabeling of neural tube explants using MMP9 (green) and HNK1 antibodies (red). Bright field view is shown in P. Dashed circle in P represents borders of NCC-migratory areas. Panel T is an enlargement of the boxed area in panel S. White arrowheads indicate MMP9/HNK1 positive NCC. Pink arrowhead represents MMP9-positive/HNK-negative NCC. Green arrowhead indicates MMP9 protein around cells. In all images, stages, treatments and staining are indicated. NT; neural tube; mes-mesoderm; ss, somite-stage; neg, negative control; NT exp, neural tube explant; NCC, migratory NCC; r, rhombomere.

delaminate in the presence of the MMP9 inhibitor in both axial levels (Figs. 2B,D,H,J); while less NCC emigrated in the presence of 5 µM MMP9 inhibitor, as compared to controls (compare Fig. 2A with B, n = 8, 10 respectively and Fig. 2G with H, n = 15, 12 respectively), a more dramatic inhibition was found in the presence of 12.5 µM inhibitor (compare Fig. 2C with D, n = 25, 20 respectively and Figs. 2I with J, n = 22, 25 respectively). Furthermore, HNK1 staining of explants shown in Figs. 2C,D,I,J revealed extensive migration of HNK1^{+}–NCC in controls (Figs. 2E,K,), compared to explants treated with MMP9 inhibitor I (Figs. 2F,L). Quantification of the inhibitory effects revealed a 4.7 fold decrease in the area of migrating NCC in the presence of MMP9 inhibitor as opposed to control value (Fig. 2U, n = 7 cultures out of 20 explants, respectively).

We next analyzed whether the effect of the MMP9-inhibitor on NCC is transient. Another set of cranial-derived explants were treated with 12.5 µM MMP9-inhibitor for overnight (12 h) and revealed prevention of NCC emigration in the treated explants (Fig. 2N, n = 5), compared to controls (Fig. 2M, n = 6), similar to the results shown above (Figs. 2G–J). However, additional incubation of these explants for 16 more hours revealed that migratory NCC began to appear around the explants that were treated with MMP9 inhibitor 28 h ago (Fig. 2P), although to a lesser extent as compared to the control explants (Fig. 2O). This result suggests that the activity of the inhibitor is reduced with time, and that the treated explants remain viable in the presence of the chemical inhibitor as evident by the retained migratory behavior.

A rescue experiment was also performed on cranial neural tube explants (Figs. 2Q–T). Following application of MMP9-inhibitor I for overnight, the inhibitory media were replaced with a control media and the explants were followed with time. Similarly to our previous results (Figs. 2G–N), NCC were prevented from detaching from the neural primordia upon addition of MMP9 inhibitor (Fig. 2R, n = 5), in contrast to control explants (Fig. 2Q, n = 5). However, the removal of the inhibitory media resulted in restoration of NCC capacity to delaminate and migrate (Figs. 2S,T). This rescue was enhanced with time, as many more cells were observed around the explants after 16 h (Fig. 2T) compared to 6 h (Fig. 2S), following the removal of the inhibitor. This assay further indicates the reversibility of the inhibitory effect of MMP9-inhibitor I and shows that prevention of NCC emigration is not due to a cytotoxic effect on the explants or loss of NCC progenitors. Taken together, the data shown in Fig. 2 demonstrates that inhibition of MMP9 prevents cranial and trunk–NCC from delaminating from the neural tube in ex-vivo conditions.

The distribution of MMP9 is evident in both emigrating and migrating NCC (Fig. 1). We thus aimed to determine whether the effect of MMP9-inhibiton is restricted only to the delamination process (as examined in Fig. 2), or whether it also affects the migration of NCC. An additional set of cranial neural tubes was explanted in ex-vivo conditions (as described in Fig. 2) and was followed as a function of time (Fig. 3). Notably, part of the explants grew in media added with the nuclear dye Hoechst to stain the living cells (Figs. 3A–D), whereas others grew in normal condition media (Figs. 3E–H). First, all explants were let to develop for 5 h without any treatment. Initial delamination and migration of cells were clearly visible around the neural tube explants, as evident in the bright-field views (Figs. 3E,F n = 8) and in the Hoechst-labeled explants (Figs. 3A-B' n = 10). Subsequently, explants were added with MMP9-inhibitor for additional 15 h and compared to controls. While control explants demonstrated a significant increase in the number of NCC around the explants and in the distance of their migration in the dish (Figs. 3C,C', G n = 8), the early-migrating NCC did not migrate much further in the MMP9 inhibited explants (Figs. 3D,D',H n = 10). In addition, there was

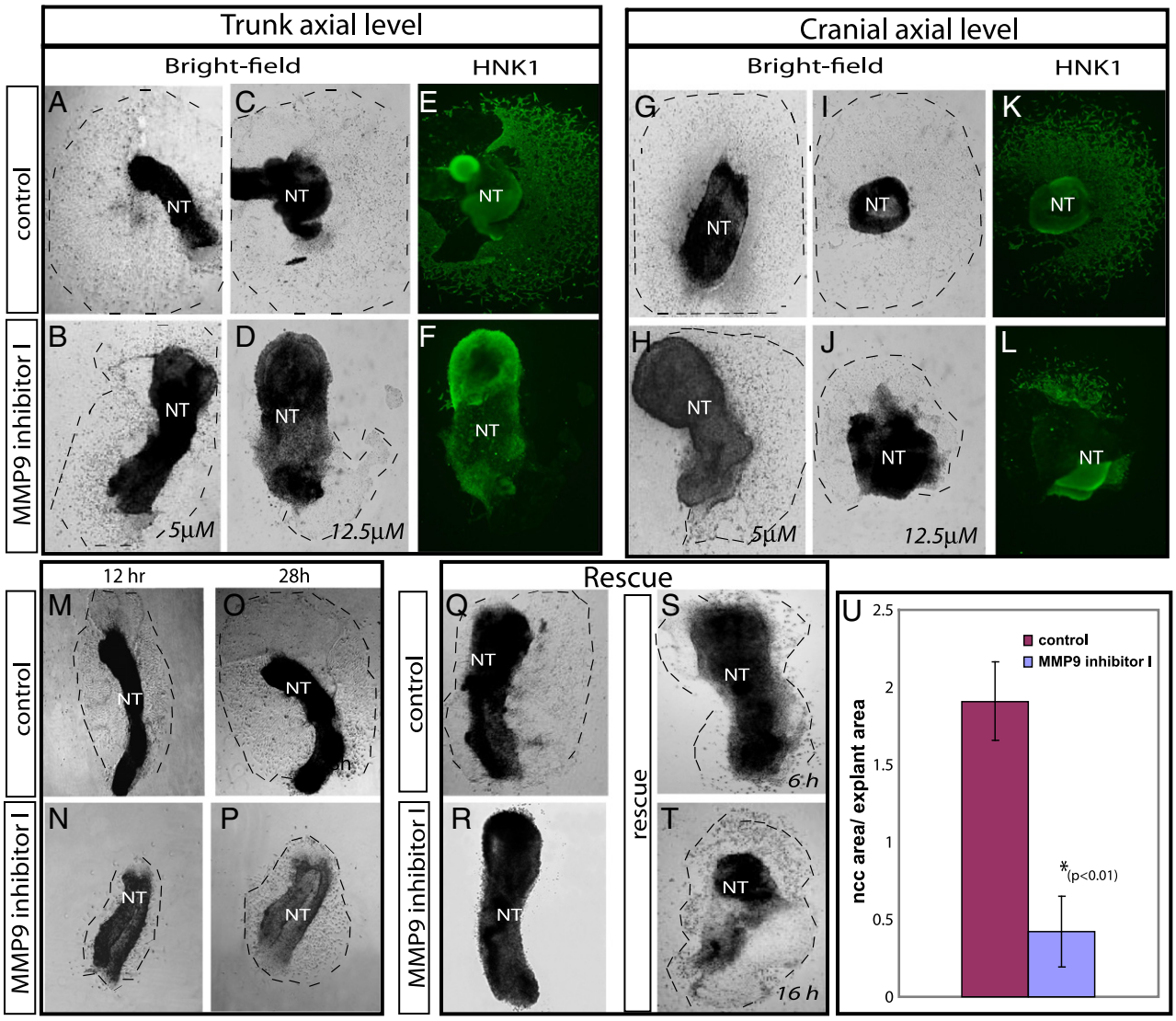

Fig. 2. Blocking MMP9 activity inhibits NCC delamination in cultured neural tubes. A–D, G–J, M–T: Bright-field images of neural tubes derived from segmental plate plus last 3 somites of embryos of 16–18 somites (A–D), or from hindbrain levels of embryos of 6–8 somites (G–J, M–T). Explants were grown for 16 h in medium containing 1% (A,G) or 2.5% (C,I, M,O) DMSO, 5 µM MMP9 inhibitor I in 1%DMSO (B,H), 12.5 µM MMP9 inhibitor I in 2.5% DMSO (D,J,N,R). (E,F,K,L): HNK1 antibody staining of explants shown in (C,D,I,J). (M–P): Control (M,O) and MMP-9 inhibited explants (N,P), treated as in (I,J) and showed after 12 and 28 h of incubation. (Q–T): Rescue of the MMP9-inhibitory effect. Explants in (Q,R) were cultured as in (I,J). (S,T): Replacement of the inhibitory media in the explant shown in (R) with control media, and evaluation of NCC migration 6 and 16 h later. (U): Quantification of the ratio between migration areas of cranial NCC to explants area, upon addition of 12.5 µM MMP-9 inhibitor versus control explants. Bars represent mean with standard deviation. Treatments, concentrations used and times of evaluations are indicated. Dashed lines represent borders of NCC-migratory areas. NT; neural tube.

much less increase in the number of cells around the neural tubes after the overnight treatment. Staining of some of these explants with HNK1 further demonstrated the sharp differences in the migration area of control versus MMP9-inhibited explants (Figs. 3I,J). Quantification of the inhibitory effect of MMP9-inhibitior on the migration of the cells showed 3 fold decrease in the area occupied by NCC in inhibited explants compared to control explants (Fig. 3K). Altogether, the data shown in Figs. 2,3 allows us to distinguish between the effect of MMP9 inhibition on delamination versus migration, and demonstrates that MMP9 inhibition prevents both the initial delamination of NCC as well as their migration. The suggested role of MMP9 in delamination and migration of NCC is in agreement with MMP9 expression patterns which are evident in the emigrating and migrating cells (Fig. 1).

To continue testing the possibility that MMP9 is required for NCC emigration, we turned to in-vivo experiments, in which the pharmacological inhibitor was injected into the neural tube. Solution containing MMP9 inhibitor I (125 µM) or DMSO was injected together with the membrane tracer CM-DiI, into the caudal neural tube of 12 somite embryos. At this stage, caudal NCC are still confined to the neural tube while more anterior cells are already undergoing migration. The addition of the DiI enabled to examine the distribution of the inhibitor along the neural tube and in the migrating NCC, which are DiI-labeled upon detachment from the neural tube. Embryos were injected twice in 4 h intervals and left to develop for 16 h. The caudally-injected MMP inhibitor I/DiI-solution extended rostrally (Fig. 4A), confirming that the inhibitor reaches trunk and cranial premigratory NCC in our experimental system. Migration of NCC was assessed by examining DiI and HNK1 staining in transverse sections obtained from an anterior (somite 5) and posterior (somite 20) axial levels (Figs. 4B–E, Table 1). In control sections obtained from anterior axial levels, migratory $HNK1^{+}/DiI^{+}$ NCC were clearly evident

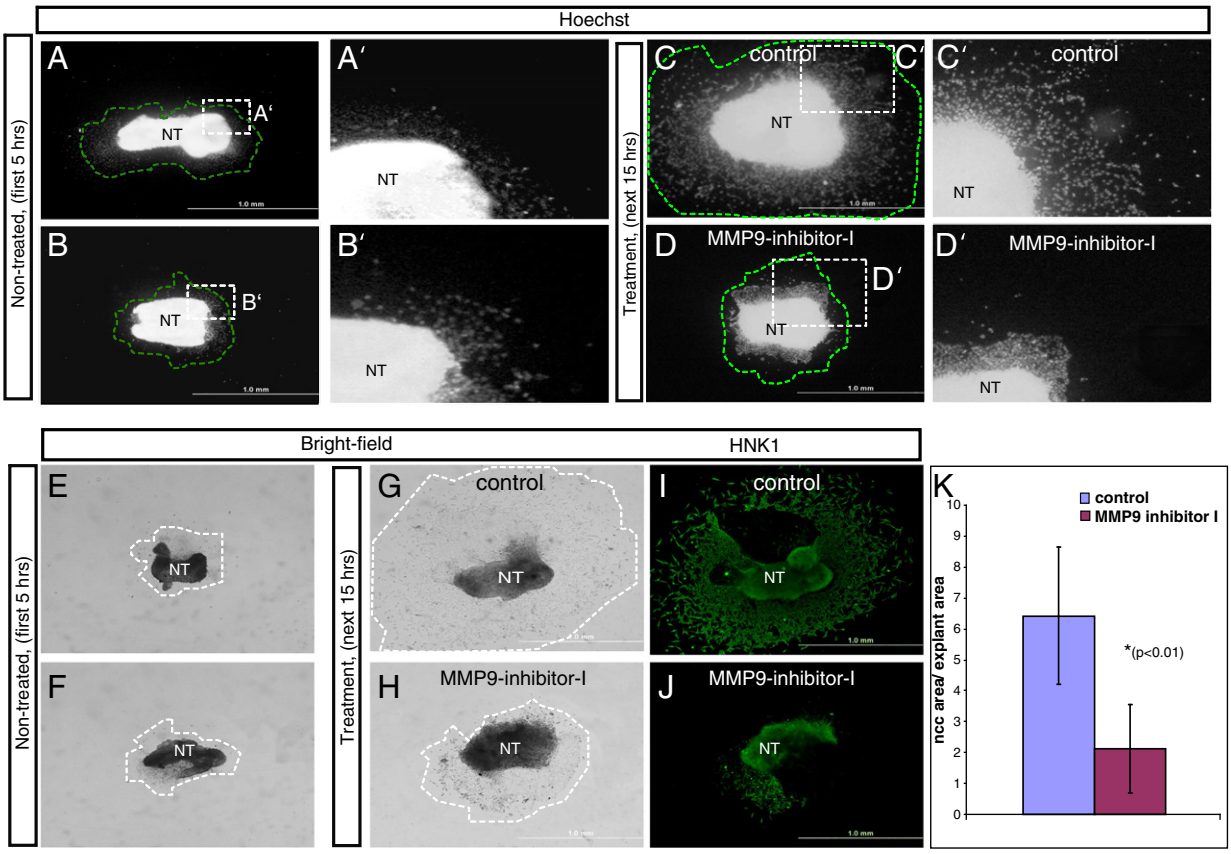

Fig. 3. Blocking MMP9 activity inhibits NCC migration in explants. Explants from hindbrain levels of embryos of 6–8 somites were grown for 5 first hours in control media (E,F) or in control media supplemented with Hoechst stain (A,B). In the following 15 h, explants were added with media containing 2.5% DMSO as control (C,G) or 12.5 μM MMP9-inhibitor I in 2.5% DMSO (D,H). (A–D): Fluorescent images of Hoechst-stained explants. Panels A′,B′,C′,D′ are enlargement of the boxed areas in panels A,B,C,D. (E–H): Bright-field images of explants. (I,J): HNK1 staining of explants in (G,H) respectively. (K): Quantification of the results obtained by measuring the ratio between migration areas of NCC to explants area and subtracting the first 5 h from overnight results. Bars represent mean with standard deviation. Treatments and times of evaluations are indicated. Dashed lines represent borders of NCC-migratory areas. NT; neural tube.

(Fig. 4B, B', n = 4). Conversely, in the MMP9-inhibited embryos almost no DiI labeling of migrating NCC was evident (Fig. 4C, C', n = 5), as well as a dramatic reduction in the migrating HNK1$^+$–NCC was found. The remaining HNK1 labeling at these rostral levels is likely to represent NCC that were already migrating when MMP9 inhibition was applied, and are thus not labeled with DiI. Similar results were found at the caudal level of the neuroaxis (Figs. 4D,E), although at this embryonic region less NCC are normally engaged in migration. Yet, while DiI$^+$/HNK$^+$ cells were evident around the neural tube in controls (Fig. 4D, D' n = 5), almost no migrating NCC were evident in the MMP9-inhibited embryos (Fig. 4E, E' n = 5). Noticeably, the red dots shown in Fig. 4E do not represent NCC, but ectodermal and neural tube stainings. Quantification of DiI$^+$/HNK$^+$ cells in control versus MMP9 inhibited embryos revealed 3.5 fold decrease in inhibited embryos.

NCC migration is a highly dynamic process which extends from as early as ~5 somites up to much later stages at different rostro-caudal levels. A previous study performed on the other gelatinase MMP2, showed that inhibition of MMP2 prevented trunk NCC from undergoing EMT at staged 12 HH (16 somites), but not at later stages (26 somites) (Duong and Erickson, 2004). Therefore, we assessed whether the effect of the MMP9 inhibition is restricted only to some stages of NCC migration, or alternatively, whether it affects NCC migration at multiple stages. The inhibitor was injected into either the cranial neuroepithelium of embryos of 5–8 somites (Figs. 4G,H) or into the caudal neural tube of 18 somite-embryos (Figs. 4I,J). In embryos injected with control solution at cranial levels, NCC migrated extensively into the head and cervix mesenchyme (Fig. 4G, n = 16). In contrast, embryos injected with MMP9 inhibitor revealed significantly weaker HNK1 staining (Fig. 4H, n = 16), especially at the posterior regions of the cranial neural tube. Serial sections taken from these embryos confirmed that many HNK1 labeled cells are seen in controls, lateral to the neural tube and during their ventral migration at midbrain and hindbrain levels (Figs. 4K,M). Conversely, a dramatic decrease in NCC migration is evident at the midbrain and hindbrain levels of embryos injected with MMP9 inhibitor I (Figs. 4L,N). Concomitantly with these results, injection of the inhibitor into caudal neural tubes resulted in a dramatic reduction of migratory NCC, seen both in whole-mounted embryos (Fig. 4J, n = 16) and in sections (Fig. 4P). In contrast, control embryos revealed typical HNK1 positive cells lateral to the neural tube, and during their migration ventrally and into rostral portions of somites (Figs. 4I,O n = 16). Altogether, these data indicate that inhibition of MMP9 prevents NCC from emigrating from the neural tube at multiple axial levels and stages.

We next used the *Foxd3* marker to further assess the effect of MMP9 inhibition on premigratory as well as on migrating NCC (Figs. 4Q–T) (Dottori et al., 2001). Normal *Foxd3* expression was evident in control embryos both in NCC progenitors that are confined to the dorsal neuroepithelium and in migrating cells (Figs. 4Q,S n = 5). In contrast, MMP9-inhibitor treated embryos showed an increase in *Foxd3* expression in the dorsal portion of the neural tube while no *Foxd3* expressing cells were found migrating (Figs. 4R,T n = 8). These results indicate that inhibition of MMP9 does not prevent NCC specification but inhibits their migration away from the neuroepithelia and confirms further our data that MMP9 inhibition prevents NCC migration in vivo and ex vivo.

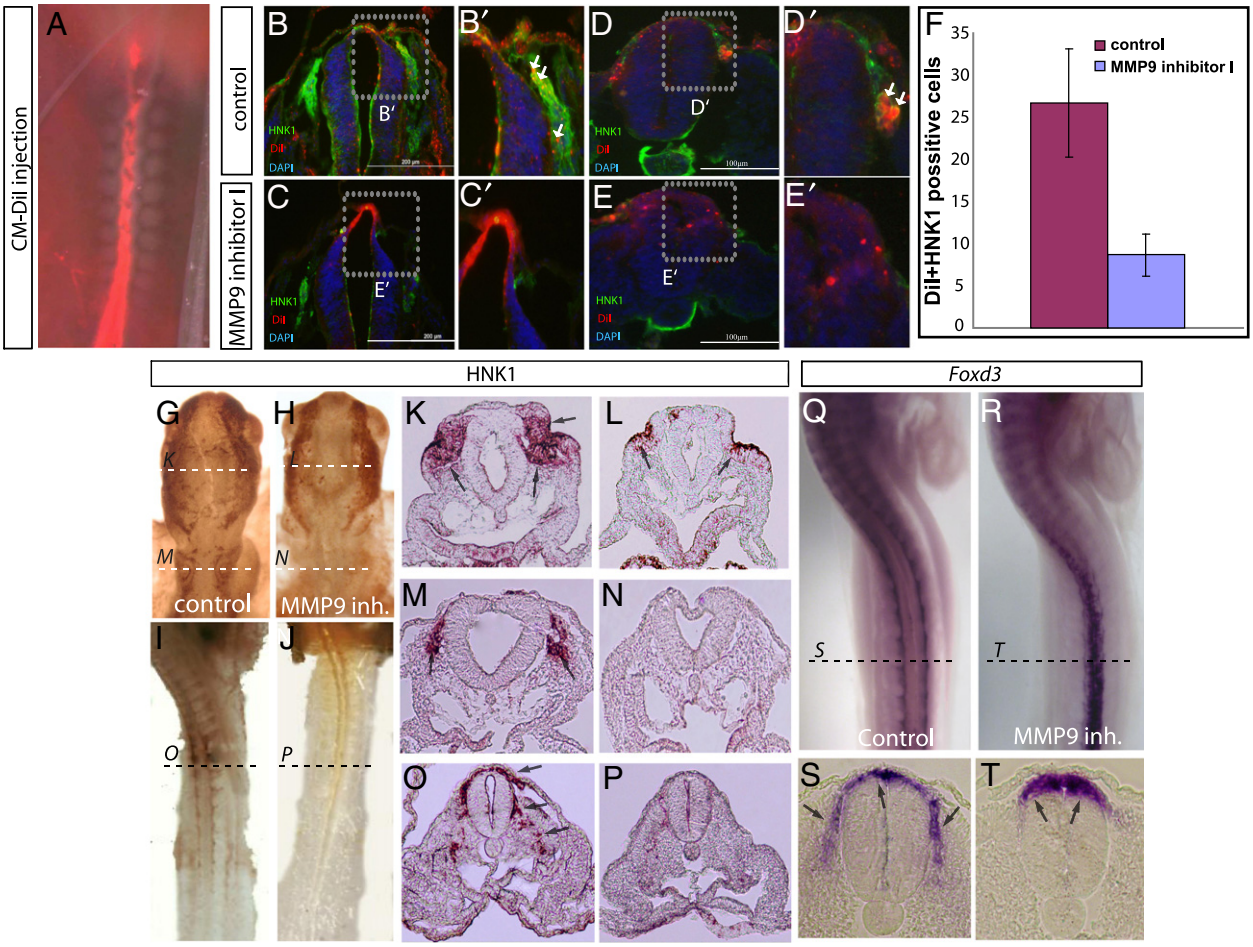

Fig. 4. Blocking of MMP9 activity inhibits NCC migration in ovo. (A): Whole-mount view of embryo injected with CM-DiI/MMP9-inhibitor I (125 μM) solution into the neural tube at the entire length of the neuroaxis of 12 somite-old embryos. (B–E): Serial sections taken from anterior (B–C) and posterior (D–E) levels of embryos injected with control (B,D) or MMP9 inhibitor I (C,E) solutions. Panels B′,C′,D′,E′ are enlargement of the boxed areas in panels B,C,D,E. Red represents DiI, green represents HNK1, blue represents DAPI staining. White arrows mark DiI and HNK1 positive cells. (F): Counts of DiI and HNK1 positive cells in control versus MMP9 inhibited embryos. Bars represent mean with standard deviation. (G–J) Whole-mount views of HNK1 stained embryos injected with control (G,I) or MMP9 inhibitor I (H,J) solutions into the neural tube at the cranial levels of 6–8 somites embryos, (G,H), or at caudal regions of embryos of 16 somites (I,J). (K–P): Serial sections taken from the dotted areas in (G–J), respectively. (Q,R): Whole-mounted embryos, treated similarly to embryos shown in (I,J,) and hybridized with *Foxd3* probe. (S,T): Serial sections taken from dotted lines in Q,R, respectively. In all images, black arrows mark HNK1 and *Foxd3* positive NCC. Treatments are indicated.

The role of MMP9 in the migration onset of NCC was next examined by an additional loss-of function approach (Fig. 5 and Table 1). FITC-conjugated morpholino-antisense oligonucleotides (MO), directed against the second exon–intron splice junction of chick MMP9 was utilized in order to produce a misspliced MMP9 mRNA (Eisen and Smith, 2008). First, the activity of the MO to knock-down the production of MMP9 was assessed by electroporating MMP9-MO or control-MO (FITC, green) into the cranial neural tube of ~6 somite-old embryos, and staining with anti-MMP9 antibody (red) 18 h later (Figs. 5A,B). In control embryos MMP9 expression was evident adjacent to the neural tube and the basement membrane around the neural tube (Figs. 5A,A′). In contrast, embryos electroporated with MMP9-MO demonstrated a marked decrease in MMP9 protein expression (Figs. 5B,B′), confirming the potency of the MMP9-MO to decrease MMP9 production. The migration of NCC was then assessed by electroporating both MO's into the mid- and hindbrain regions of ~5 somite-old embryos (Figs. 5G,H) or into the caudal neural tube of 18 somite-old embryos (Figs. 5C,D). Immunostaining against HNK1 (orange) and FITC-MO (blue) was performed 18 h later. Control embryos demonstrated typical HNK1-positive NCC that migrate at the head and trunk axial levels (Figs. 5C,G, n = 12 for each), at both the electroporated and the contra-lateral sides of the neural tube. A significant reduction of HNK1-stained cells was evident in embryos expressing MMP9-MO, both at the cranial and trunk levels of the neuroaxis (Figs. 5D,H n = 12 for each). These results were also confirmed by HNK1-labeling of transverse sections taken from control (Figs. 5E,I) and MMP9-MO (Figs. 5F,J) embryos. Notably, the effect of MMP9-MO was observed on both sides of the neural tube. This may be a result of MO-electroporation occurring at much lower levels also at the contra-lateral neural tube that is harder to detect in our system (Figs. 5E,F,I,G), see also Weisinger et al. (2008). Alternatively, as MMP9 is a secreted protein that acts at the ECM in a limiting concentration, it is highly possible that its knockdown causes it to be less available also in areas outside of the knockdown cells. These results are further confirmed in the embryos stained with MMP9 antibody (Figs. 5A,B), in which reduction of MMP9 expression is also visible in larger areas than the MMP9-MO electroporated regions. To further confirm the requirement of MMP9 for migration of NCC, we performed a rescue experiment (Figs. 5K–P), by electroporation of MMP9-MO followed by injection of MMP9-enriched media into the neural tube (see Figs. 6,7 for details about MMP9-conditioned media and their effect on NCC migration). Our results show retention of migratory NCC in the rescue experiment, as revealed by HNK1 staining (Figs. 5M,P, n = 6), as compared to the MMP9-MO (Figs. 5L,O n = 7) and control (Figs. 4K,N, n = 7) embryos. This result supports our previous findings and rules out the possibility of a toxic effect of the MO treatment. Moreover, the increase in HNK1-positive cells in rescued embryos

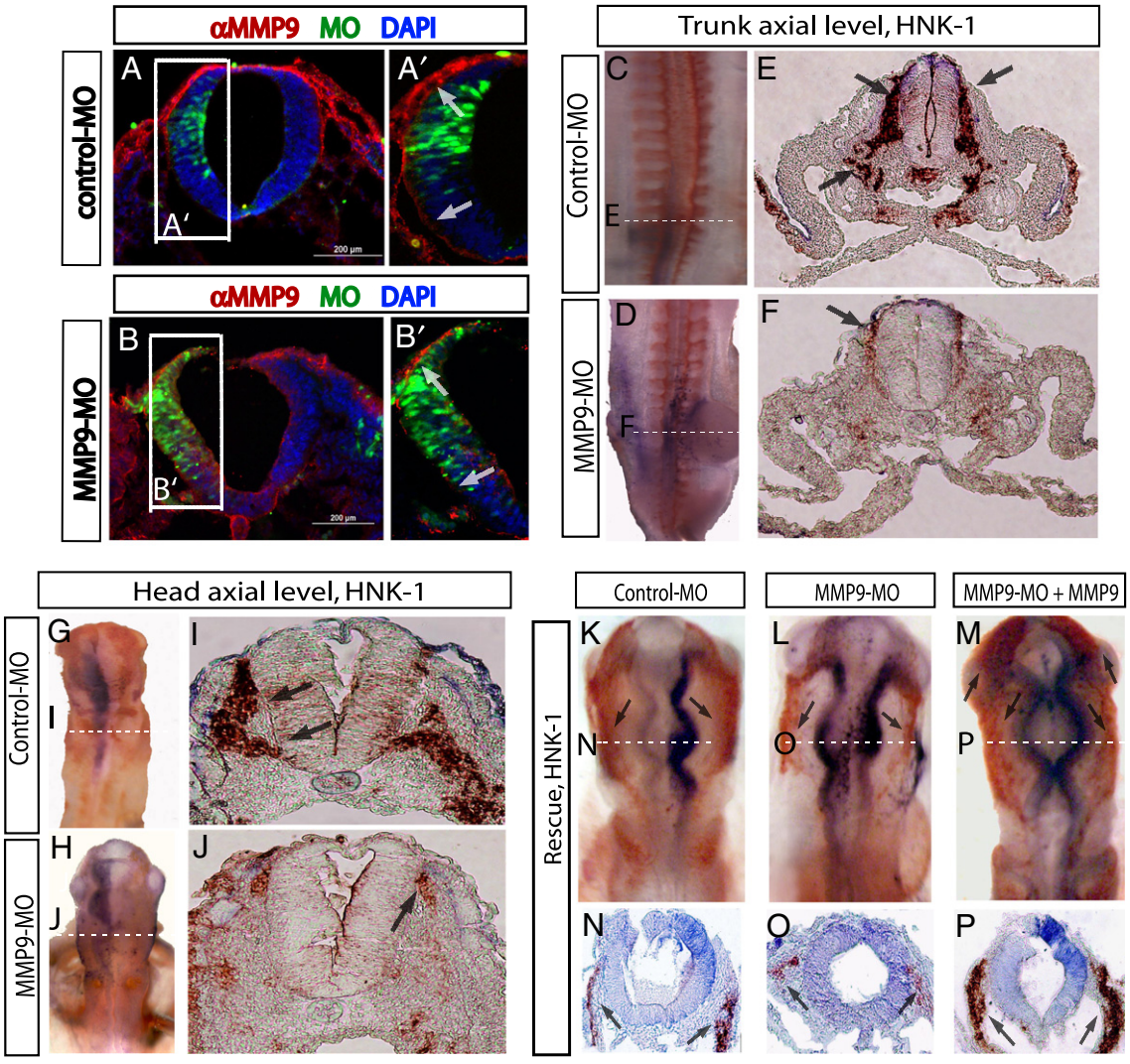

Fig. 5. Electroporation of MMP9-MO prevents NCC migration. (A–B): Transverse sections taken from embryos electroporated at the stage of 6 somites with FITC-conjugated control-MO (A) or MMP9-MO (B) and labeled with MMP9 antibody. Red and green staining shows MMP9 and MO-expressing cells, respectively, blue represents DAPI stain. Images in A′,B′ are enlargements of the boxed areas in A,B. (C,D,G,H,K–M): Whole-mount images of HNK1 stained embryos, electroporated at the stage of 18 somites (C,D) or 5 somites (G,H,K–M) with FITC-conjugated control-MO (C,G,K) or MMP9-MO (D,H,L,M). Embryo in (M) was injected with MMP9-enriched media 6 h after the electroporation. (E,F,I,J,N–P): Serial sections taken from the dotted lines in (C,D,G,H,K–M), respectively. Brown and blue stains show HNK1 and MO-expressing cells, respectively. In all images, treatments are indicated. Black arrows mark HNK1 positive NCC, white arrows mark MMP9 staining.

compared to control is in agreement with results obtained in MMP9 gain-of-function experiments (see Figs. 6–7). To additionally eliminate the possibility of a non-specific effect of the MMP9-MO, we tested whether it affects cell proliferation and cell death in the neural tubes. Electroporation of both control-MO and MMP9-MO did not affect the mitotic divisions of cells at each side of the neural tube, as shown by anti-pH3 staining (Supplementary Fig. 1), nor did it reveal any excessive cell death, as shown by TUNEL assay (Supplementary Fig. 1). Together, these results support our previous experiments (Figs. 2–4) and confirm that MMP9 is required for NCC delamination and migration at multiple axial levels and embryonic stages.

Addition of exogenous MMP9 induces enhanced migration of NCC

We next studied whether exogenous MMP9 will enhance NCC migration from the neural primordia. To generate a tool to increase MMP9 activity, we established a cell line of rat chondrosarcoma (RCS) constantly expressing MMP9. Chick MMP9 cDNA, including the signal peptide, binding and catalytic sites of MMP9 and excluding the c-terminal hemopexin regulatory domain, was cloned into pCDNA3 construct and transfected into RCS cells that were selected for MMP9 stable production (Ben-Zvi et al., 2006; Weizmann et al., 2005). The gelatinolytic activity of the MMP9 was demonstrated in cell lysates and cultured media, using gelatin impregnated zymography gel (Figs. 6A,B). This assay confirms that the cells express the transfected 40 kDa MMP9 which is secreted into the media as an active enzyme. The increasing levels of active MMP9 were found in the media, but not in cells, as expected for secreted MMP (Figs. 6A, B). An additional 62 kDa band is also observed in both control and MMP9-transfected cells, corresponding to the endogenous MMP2, which is expressed at low levels in RCS cells (Tong et al., 2003).

Conditioned media from control or MMP9-transfected cells were added to neural tube explants, isolated either from posterior segmental plate or from hindbrain levels of 16 or 6 somite-old embryos, respectively (Figs. 6C–J, Table 1). As expected following 16 h of incubation, NCC delaminated and migrated in control explants of both head and trunk regions, as shown in bright-field images as well as following HNK1 staining (Figs. 6C,E,G n = 15 for each region, respectively). Addition of MMP9-media significantly enhanced the outgrowth of NCC from cranial and trunk neural tubes (Figs. 6D,F,H n = 16 for each region, respectively). Quantification of these results revealed 1.4 fold increase in the area of migrating NCC in the presence of excess MMP9 as

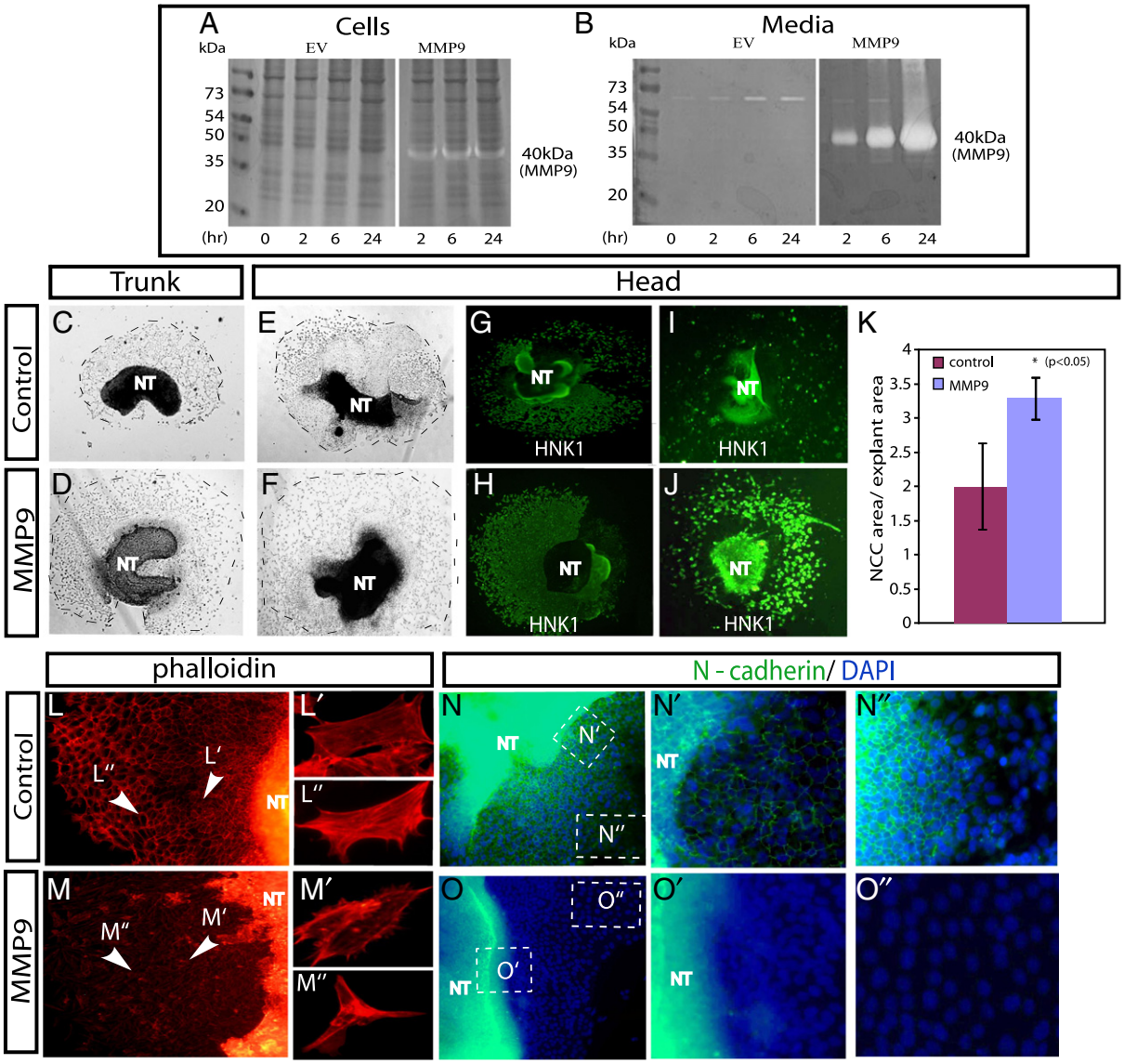

Fig. 6. Enhanced EMT and migration of NCC in explants treated with excess MMP9. (A,B): A rat chondrosarcoma cell line (RCS) was transfected with an empty pCDNA3 vector (EV) or with a vector containing avian 40 kDa MMP9 insert (MMP9). At the indicated times, samples of cells (A) or conditioned media (B) were collected and analyzed under non-reducing conditions on gelatin zymography. Bands corresponding to the endogenous 62 kDa MMP2 and the transfected 40 kDa MMP9 are detected. (C–F): Bright field images of isolated neural tubes from segmental plate levels of 16 somite-old embryos (C,D) or hindbrain levels of 6 somite-old embryos (E–F) that were seeded onto fibronectin-coated dishes and grown 16 h in control RCS media (C,E), or in MMP9-containing RCS media (D,F). Dashed circles represent borders of NCC migration area. (G–J): HNK1 antibody staining of explants derived from hindbrain levels of 6 somite-old embryos that were either grown on fibronectin coated dishes with control (G) and MMP9-media (H) or seeded on top of control RCS (I) and MMP9 RCS (J) cell layers. (K): Quantification of migrating cranial NCC area upon addition of MMP-9 media versus control explants. Bars represent mean and standard deviation. (L–M″): Explants treated with control (L) or MMP9-enriched media (M) and stained with phalloidin. Images in L′,L″,M′,M″ are enlargements of areas marked in L,M by white arrowheads. (N–O″): Explants treated with control (N) or MMP9-media (O) that were examined for N-cadherin distribution at cell membranes. Images in N′,N″,O′,O″ are enlargements of boxed areas in N,O. Green represents N-cadherin and blue represents DAPI stain. In all images treatments are indicated. NT; neural tube.

compared to control values (Fig. 6K, n = 10 cultures out of 15 explants for each treatment). In a parallel approach neural primordia isolated from cranial levels were explanted on top of control or MMP9-producing RCS cell layers. The explants were labeled with HNK1 16 h later (Figs. 6I,J). In general, the migration of NCC on top of RCS cells was less efficient, as compared to fibronectin-coated dishes. Yet, a large amount of cells expressing HNK1 were found around the explants seeded on top of MMP9-secreting cells (Fig. 6J, n = 5), while much fewer HNK1^{+}-cells grew on control RCS (Fig. 6I, n = 5). Notably, in both types of experiments, excess MMP9 did not affect the integrity of the neural tubes (Figs. 6C–J), indicating that MMP9 acts specifically to enhance NCC migration rather than to induce general protein degradation and dissociation of cells in culture.

The effects of MMP9 were also examined on the epithelial/mesenchymal characteristics and shape of the excessively migrating NCC. Staining with phalloidin, that binds to the actin filaments of the cytoskeleton (Groysman et al., 2008; Wright et al., 1988), reveled the typical organization of stretched stress-fibers in migratory NCC around the control explant (Figs. 6L–L″ n = 18). However, the organized structure of stress-fibers was perturbed in NCC migrating in MMP9-treated explants (Figs. 6M–M″ n = 14), suggesting accelerated loss of epithelial morphology upon excess MMP9 and transition toward mesenchymalization. Epithelial properties of the cells were also examined by staining for N-cadherin, an adhesion molecule known to accumulate at the apical membrane of neuroepithelial cells and to be downregulated in mesenchymal cells (Groysman et al., 2008; Nakagawa and Takeichi, 1998; Shoval et al., 2007; Taneyhill, 2008). Staining of control explants revealed a typical N-cadherin localization in NCC membranes that migrated around the neural tube (Figs. 6N–N″, n = 12), and its absence in cells that moved further away from the explant (Fig. 6N″). In

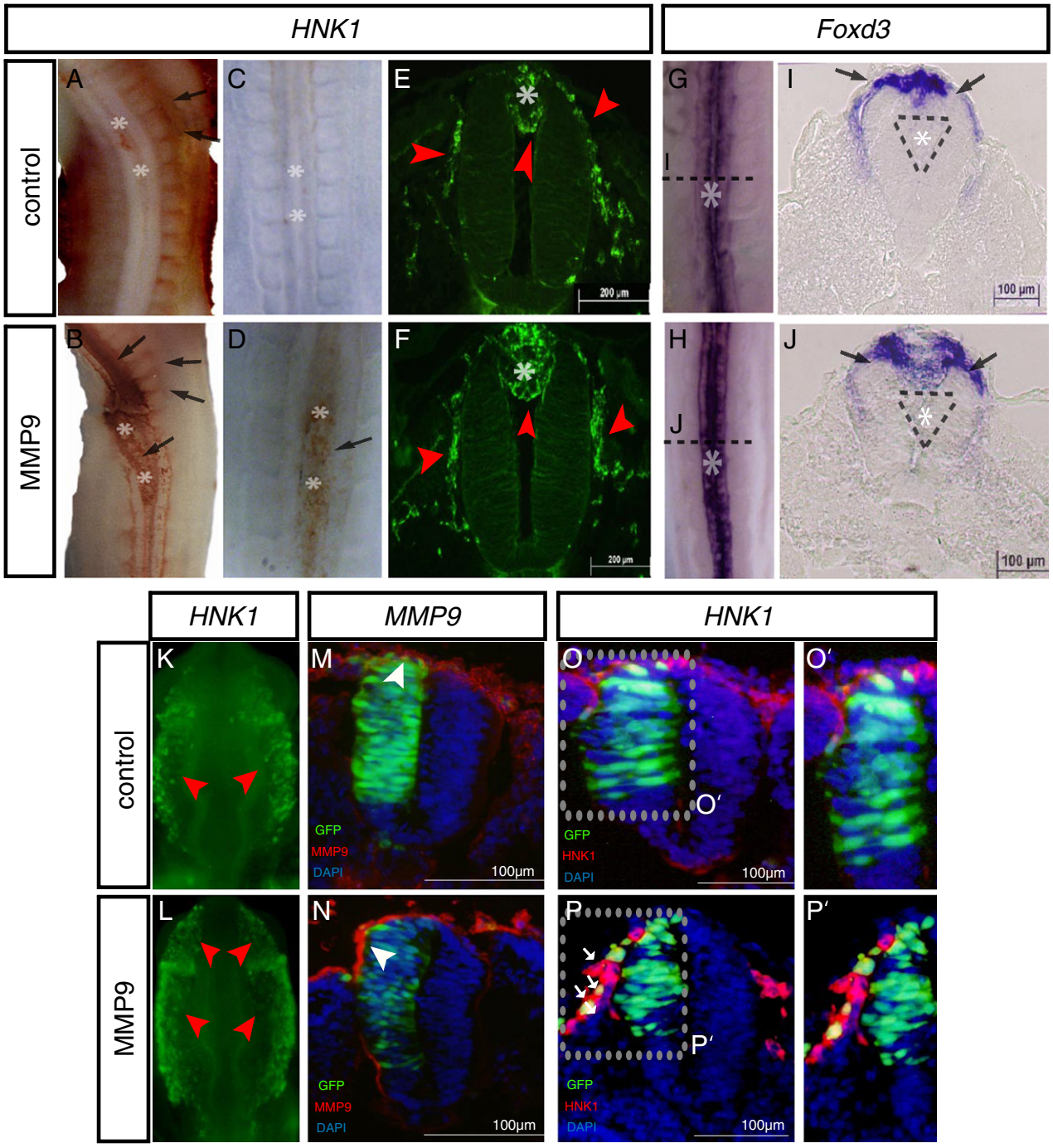

Fig. 7. MMP9 induces enhanced and precocious NCC migration in vivo. Whole mount views or transverse sections of embryos grafted with control (A,C,E,G,I) or MMP9-expressing RCS cells (B,D,F,H,J). Cell pellets were grafted dorsal to the neural tube at anterior (A,B,E,F,G,H) or posterior (C,D) segmental plate levels. Embryos were incubated for 18 h, and processed for HNK1 immunostaining (A–F) or for in situ hybridization with *Foxd3* probe (G–J). Transverse sections in (I,J) are taken from dotted lines in (G,H). (K,L): Whole mount views of embryos injected with control (K) or MMP9-conditioned media (L) and stained for HNK1 6 h later. (M–P): Serial sections taken from control embryos expressing pCAGGS-IRES-GFP vector (M,O) or pCAGGS-MMP9-IRES-GFP vector (N,P). Embryos were stained with MMP9 (M,N) or HNK1 (O,P) antibodies (red). In (M–P) green represents electroporated cells, blue represents DAPI stain. Images in O',P' are enlargements of boxed areas in O,P, respectively. In all images, treatments are indicated, grafted cells are marked with an asterisk, black and white arrows and red arrowheads mark NCC, white arrowheads mark MMP9 expression.

contrary, no N-cadherin was evident in the migratory NCC of the MMP9-treated explants, regardless of their distance from the neural tube (Figs. 6O–O″, n = 7). Together, these data demonstrate that MMP9 is indeed sufficient to enhance NCC separation and migration in ex-vivo explants as evident by the increased areas of migrating NCC and by their switch from epithelial-to-mesenchymal morphology.

To verify these findings in whole embryos, control or MMP9-secreting RCS cells were grafted at, and adjacent to, the dorsal neural tube of embryos of 16–18 somites, at levels corresponding to the anterior segmental plate (Figs. 7A,B and Table 1). These axial levels consist of specified NCC prior to their onset of migration (Cheung et al., 2005; Sela-Donenfeld and Kalcheim, 1999, 2000, 2002). Embryos were assessed for NCC migration 18 h later, a stage when NCC are expected to delaminate from the neural tube into the paraxial mesoderm. Analysis of HNK1 staining in control embryos revealed typical migratory patterns of NCC adjacent to the neural tube and at the rostral portion of somites, at the graft levels (Fig. 7A, n = 10). Notably, some HNK1 staining is also located around the graft, indicative for

NCC that may bypass the graft during emigration. In a sharp contrast, massive accumulation of cells expressing HNK1 is found around and within the MMP9-cell graft (Fig. 7B n = 8). Transverse sections were performed from similarly-treated embryos at the level of the mid-trunk, followed by HNK1 staining (Figs. 7E,F). In agreement with the whole-mounted embryos (Figs. 7A,B), NCC were already migrating in embryos receiving control graft (Fig. 7E). Yet, more HNK1 positive cells were evident in embryos grafted with MMP9-expressing cells (Fig. 7F). We next examined whether MMP9 can elicit a precocious delamination of cells at more posterior axial levels, where NCC are still expected to be confined to the dorsal neural tube at the time of fixation (Sela-Donenfeld and Kalcheim, 2000). MMP9 or control cells were implanted at the level of posterior segmental plate and assessed for HNK1 staining after 14 h, such that the graft will be positioned adjacent to epithelial somites (Figs. 7C,D). No HNK1 staining was evident around the control graft, but only at more anterior axial levels, as expected by this embryonic stage (Fig. 7C n = 3). However, embryos grafted with MMP9 cells showed high levels of HNK1 staining around the caudal graft (Fig. 7D n = 3), further implying that MMP9 can induce a premature outgrowth of NCC progenitors. Notably, most of these cells accumulated around the graft, rather than migrating toward the paraxial mesoderm. This may result from the posterior axial level that may not yet be permissive for NCC migration or from the premature state of NCC. Next, another set of control or MMP9-treated embryos was examined for the distribution of *Foxd3* (Figs. 7G–J). Embryos grafted with control cells showed *Foxd3* distribution in a normal pattern mostly at the dorsal neural tube, as expected at the time of fixation (Figs. 7G,I n = 4). MMP9-grafted embryos showed an increase in *Foxd3*-expressing cells at, and around, the dorsal neuroectoderm (Figs. 7H,J n = 5).

To further confirm these results we took two additional approaches; first, pCAGGS plasmids encoding for GFP or MMP9-IRES-GFP cDNAs were electroporated into the neural tubes of 6–8 somite old embryos. Embryos were analyzed 16 h later for MMP9 expression and NCC migration. Excess levels of MMP9 protein were clearly demonstrated in the hemi-neural tubes transfected with MMP9 cDNA (Fig. 7N), in contrast to the contra-lateral side of the neural tube or to controls (Fig. 7M), which demonstrated normal MMP9 patterns (see also Fig. 1J). Concomitantly, MMP9-expressing embryos demonstrated a marked increase in NCC migration (Figs. 7P,P′ n = 7), when compared to control embryos (Figs. 7O,O′ n = 8). Furthermore, we injected conditioned-media (see Fig. 6) into the neural tube lumen and assessed whether enhancement in NCC migration is rapidly evident. Embryos of 8 somites were injected twice at the cranial regions and harvested 6 h later, at the stage of 12 somites, followed by staining with HNK1 (Figs. 7K,L). Typical migration of NCC was evident in embryos receiving control media, as expected by the time of fixation (Fig. 7K n = 10). Nevertheless, an increase in HNK1 positive NCC was observed in embryos receiving MMP9-media (Fig. 7L n = 11). This augmentation was more expanded compared to the grafting method, as expected by the solubility of this enzyme. Altogether, the results presented in Fig. 7 and Table 1 indicate by multiple means that excess MMP9 is sufficient to enhance NCC migration from the neural tube in vivo.

Mechanism of activity of MMP9 in promoting NCC emigration from the neural tube

As MMP9 is an enzyme capable of degrading wide range of substrates (Hahn-Dantona et al., 2000), it is tempting to speculate that at least some of its underlying mechanisms of action in NCC involve the direct degradation of adhesion molecules, such as N-cadherin and basal membrane components, such as laminin. Loss of both proteins, from the dorsal neural tube or dorsal basement membrane, respectively, is evident during NCC onset of migration (Duband and Thiery, 1987; Erickson, 1988; Perris et al., 1989). In order to examine these possibilities, isolated neural tube explants were cultured for 16 h, to enable normal NCC delamination and migration. Then, conditioned media from control or MMP9-transfected cells were added to the explants for 0.5 and 3 h, prior to fixation (Figs. 8A–H, n = 9 for each time point). These short incubation periods are expected to reflect modifications in processes such as proteolysis, rather than in gene expression level and cell differentiation. As expected, there were no differences in the migration distance between the treatments, since the MMP9 was added only after NCC were already migrated away from the explants (Figs. 8A,C,E,G). Nevertheless, a remarkable reduction in N-cadherin staining of NCC adjacent and around the neural rubes was evident already after 30 min of incubation with MMP9-condition-media (Figs. 8D, D′), while the typical epithelial N-cadherin staining was observed in NCC adjacent to the neural tube of control explants (Figs. 8B,B′). The same results were obtained after 3 h of incubation (Figs. 8F,H). Notably, N-cadherin was still present within the neural tubes of MMP9-treated explants (Figs. 8D,H and Fig. 6O), indicating that MMP9 effect on N-cadherin is most noticeable in NCC. Possible mechanisms for these differential effects are elaborated in the Discussion section. Intriguingly, we observe the appearance of fluorescent staining in the explants treated with MMP9 which are not localized to cell surface but accumulate in between the cells, or in a dotted fashion around the cell membrane. These findings further suggest that MMP9 directly degrades this protein which may facilitate cell motility. Together, these data suggest that N-cadherin may be a direct substrate of MMP9 in ex-vivo explants.

In the next step we aimed to analyze the possible substrates in-vivo by gain-and-loss-of-function manipulations, in which control media (Figs. 8I,M,K,O), MMP9-media (Figs. 8J,N) or MMP9 inhibitor I (Figs. 8L,P) were injected into the neural tube lumen of 5–7 somite-staged embryos, as described in Figs. 4,7. Embryos were incubated for 15 h, fixed, sectioned and immunostained for N-cadherin or laminin. In agreement with the results obtained in the explants (Figs. 8A–H), N-cadherin expression was decreased from a larger domain of the dorsal neural tube in MMP9-treated embryos at axial levels where NCC migration takes place (Figs. 8J–J″ n = 6), compared to control embryos (Figs. 8I–I″ n = 6). Notably, expression of N-cadherin that normally surrounds the entire apical lumen of the neural tube was also partially-degraded upon the addition of MMP9 (Figs. 8J,J″ compared to I,I″). However, the inhibition of MMP9 revealed no differences in the region of the dorsal neural tube that lacked N-cadherin (Figs. 8L,L′ n = 8) as compared to control (Figs. 8K,K n = 8). These data suggest that although N-cadherin may be one of the substrates of MMP9 in vivo (Zheng et al., 2009; Zuo et al., 2011), MMP9 is not the main enzyme responsible for the degradation of N-cadherin, as it is still degraded from the dorsal neural tube in MMP9-inhibitory conditions. Indeed, previous results demonstrated that the Adam protease is mediating N-cadherin degradation in the dorsal neural tube (Shoval et al., 2007).

The same experimental setting was used to analyze the ability of MMP9 to degrade laminin, a major protein of the basal-lamina that becomes scattered from the dorsal neural tube at stages of NCC migration, to form a narrow passage for the NCCs (Desban et al., 2006; Tzu and Marinkovich, 2008). Immunostaining for laminin demonstrated the typical staining surrounding the neural tube with a gap at the dorsal part of the neural tube in control embryos (Figs. 8.M, M',O,O' n = 12). A clear widening in the laminin negative region at the dorsal part of the neural tube was evident upon addition of MMP9 (Figs. 8 N,N′ n = 10). Conversely, the gap in laminin expression in the dorsal neural tube was not evident when the enzyme was inhibited (Figs. 8P,P′ n = 10). These results suggest that MMP9 enhances breakage of laminin at the basement-membrane to enable NCC emigration from the neural tube, indicating that laminin is one of MMP9 native substrates which its degradation contributes to execute the process of NCC migration.

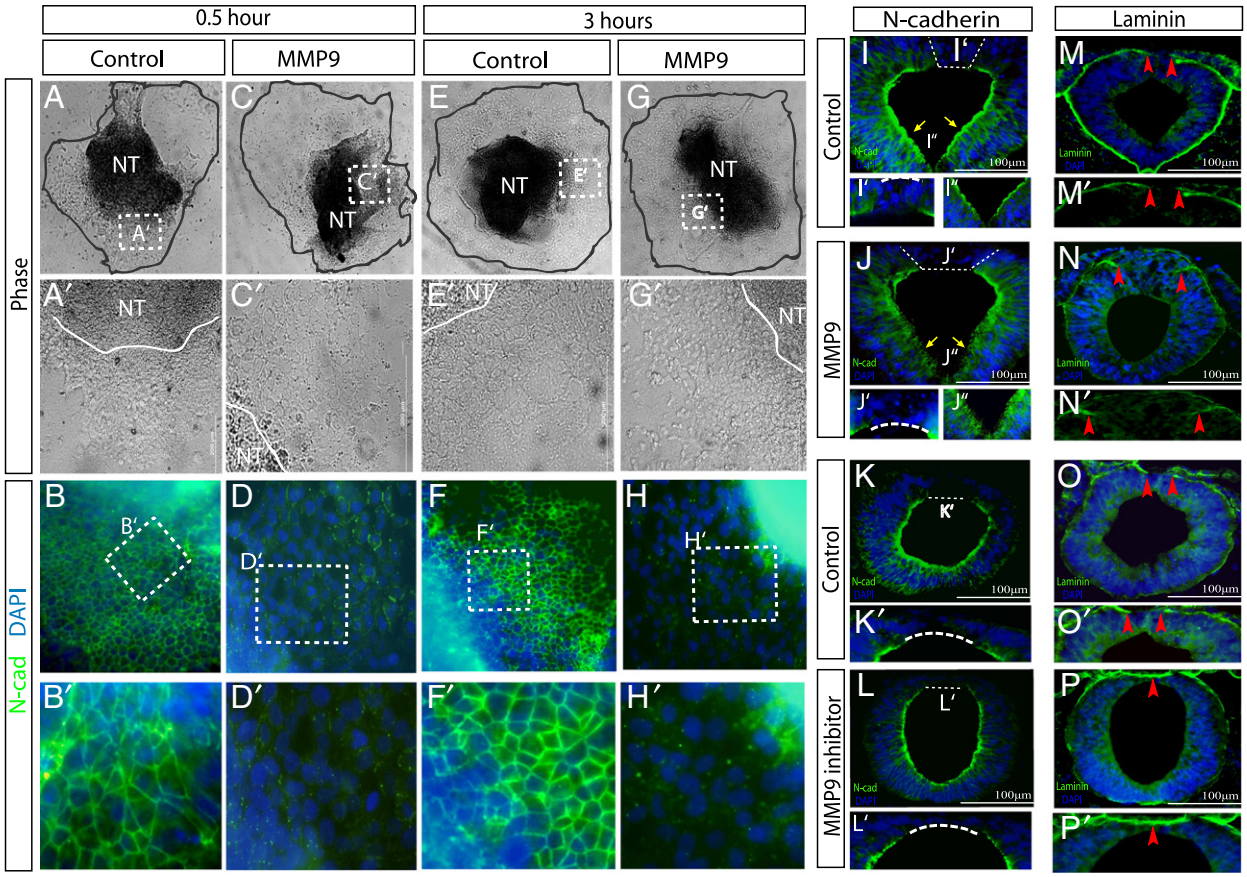

Fig. 8. N-cadherin and laminin are substrates for MMP9 in NCC. (A–H): Bright field images (A,C,E,G) and fluorescent images of N-cadherin antibody staining (green; B,D, F, H) of isolated neural tubes seeded onto fibronectin-coated dishes and grown 16 h, followed by addition of control RCS media (A,B,E,F) or MMP9-containing RCS media (C,D,G,H) for 0.5 h (A,B,C,D) and 3 h (E,F,G,H). Gray circles represent borders of NCC migration area, white lines represent borders of neural tubes. Images in (A′–H′) are enlargements of boxed areas in (A–H). (I,J,M,N): transverse sections of embryos injected with control (I,M) or MMP9-conditioned media (J,N) as described in Fig. 7. (K,L,O,P): Transverse sections of embryos injected with control (K,O) or 125 μM MMP9 inhibitor I (L,P) solutions, as described in Fig. 4. Sections were stained with N-cadherin (I–L) or laminin (M–P) antibodies. Dashed lines mark the gap between N-cadherin expressing areas, yellow arrows indicate N-cadherin positive cells in the NT, and red arrowheads represent the gap in laminin expression in the basement membrane. Images in I′–P′ are enlargements of marked areas in I–P respectively. In all images, blue represents DAPI stain and treatments are indicated. NT; neural tube.

Discussion

This study asked whether MMP9 is involved in the processes of NCC detachment from the neural tube and migration. We show MMP9 mRNA and protein expression at stages and sites where trunk and cranial NCC delaminate and migrate. Inhibition of MMP9 in NCC by different approaches and at different levels of the neural axis eliminates NCC delamination and migration, while exogenous MMP9 enhances and precedes their detachment from the neuroectoderm and converts the cell morphology into mesenchyme. Assessment of possible substrates for MMP9 reveals that MMP9 is capable to cleave both N-cadherin from NCC membranes and laminin from the basement membrane around the neural tube, acting predominantly on degrading laminin. Together, these results (summarized in Table 1) show for the first time that MMP9 has a major role in executing the EMT and migration of NCC.

MMP9 is central to many EMT, cell invasion and tissue-remodeling processes in adults and in cell-culture systems (reviewed in Vu and Werb, 2000). During embryogenesis, MMP9 serves mainly as a marker in events where ECM remodeling is taking place, such as during angiogenesis, heart and limb development (Malemud, 2006a, b; Shelton and Yutzey, 2007; Simsa et al., 2007a). However, almost nothing was shown regarding the function for MMP9 during development, although EMT, cell migration and ECM-modifications constantly occur. Recent data from *Xenopus* embryos revealed that MMP9, -7 and -18 are expressed in early macrophages and are required for their migration prior to the establishment of the circulatory system (Tomlinson et al., 2008). MMP9 was also suggested to be involved in pancreatic islet formation during the migration of endocrine cells (Perez et al., 2005), as well as during kidney morphogenesis (Lelongt et al., 1997). Later in development, MMP9 possibly acts during odontogenesis, where EMT, motility and active remodeling of the dental primordia take place (Randall and Hall, 2002). Moreover, during mandibular arch development, MMP9 was found in the cartilage tissues together with MMP13, where a general inhibition of both resulted in dramatic defects in Meckel's cartilage (Chin and Werb, 1997; Miettinen et al., 1999; Shimo et al., 2004). Notably, while cranial NCC significantly contribute to tooth and mandible formation, these studies did not examine whether the described defects are linked to MMP's roles in NCC. Our data shows for the first time not only that MMP9 is expressed in early NCC, but that it has a functional role in executing their emigration from the neuroectoderm by degrading laminin, and possibly N-cadherin. MMP9 role in early NCC stages may very well be conserved also at the later stages of NCC development. Therefore, future studies are required to assess the expression and function of MMP9 in later NCC-related structures, such as in the branchial arches, heart and dorsal root ganglia. In addition to the NCC themselves, MMP9 was found to be expressed in their migratory paths. This may implicate that NCC surrounding environment may also produce MMP9 to promote their migration,

and/or that MMP9 has broader functions in the embryo, on top of its role in NCC. Yet, MMP9 silencing within NCC was sufficient to prevent their migration, which suggests that a major source of MMP9 production and action resides in NCC.

Intriguingly, MMP9 null mice are viable without any clear embryonic defect (Vu et al., 1998). These mice exhibit delayed ossification of the post natal growth plate due to inhibition of angiogenesis and apoptosis in the hypertrophic chondrocytes (Engsig et al., 2000; Sternlicht and Werb, 2001). In addition, mice lacking MMP9 show reduced tumor invasiveness and metastasis formation, in agreement with the activity of this gelatinase in tumor aggressiveness (Coussens et al., 2000; Itoh et al., 1999). Due to the limited data available regarding MMP9 expression in embryonic mouse neural tube (Canete-Soler et al., 1995), it is necessary to examine whether the MMP9 patterns observed in NCC in early avian embryos are also conserved in mammals, and thus, the lack of any developmental phenotype in the mutants may be due to redundancy with other MMPs.

Indeed, previous data have shown that *MMP2* is expressed in chick NCC within the pharyngeal arch mesenchyme and during their migration to the heart (Cai et al., 2000), and that MMP2 inhibition prevented cardiac NCC migration (Cai and Brauer, 2002). Another relevant study (Duong and Erickson, 2004) found *MMP2* to be transiently expressed in delaminating NCC at the dorsal neuroectoderm and that it is rapidly extinguished as they disperse. Conversely, our data show that MMP9 mRNA and protein are detected in the detaching as well as in the migrating cranial and trunk NCC, suggesting an ongoing role for MMP9 in this process, in contrast to MMP2 which is more restricted to the EMT. Further support for this assumption comes from MMPs inhibition; while application of MMP2-MO prevented EMT but did not affect motility of cells that already delaminated from the neural tube (Duong and Erickson, 2004), our knocking-down of MMP9 activity showed a more robust prevention of NCC delamination and migration. This effect occurs at several axial levels, including regions where NCC are still confined to the neural tube at the time of treatment as well as domains where they are already undergoing delamination. Notably, some of the chemical inhibitors used in the previous studies to prevent NCC emigration (Cai and Brauer, 2002; Cai et al., 2000; Duong and Erickson, 2004), are capable to inhibit several MMPs, including MMP9, further corroborating our findings regarding an important role of MMP9 in NCC. Whether a communal or a single activity of these gelatinases accounts for NCC migration events in avian embryos is still an open question. Moreover, other members of the MMP family that have also been identified in NCC (MMP14,-16, data not shown) may also contribute to these processes.

Mutations in MMP2 were found in human (Al Aqeel et al., 2000; Al-Aqeel, 2005; Al-Mayouf et al., 2000; Martignetti et al., 2001). These mutations manifest a disorder involving characteristic ECM-degradation pathologies including facial features. MMP2 null mice (Itoh et al., 1997) are viable, but display several mild defective bone and cartilage tissues (Mosig et al., 2007), in some agreement with the human mutation. Notably, cranial defects found in the MMP2 human mutation were also observed in the MMP14-null mice (Holmbeck et al., 1999). As MMP14 is an activator of MMP2 (Kinoh et al., 1996; Zhou et al., 2000), it is possible that a deficiency in either of these enzymes can lead to a common pathology. As mentioned above, our preliminary data suggest that MMP14 is also expressed in avian NCC, supporting further this possibility. Similar to the unclear expression or role of MMP9 in mammalian NCC, whether MMP2 is expressed in mouse NCC is also still elusive (Reponen et al., 1992), and whether the above mentioned phenotypes result due to NCC defects, is unknown. Based on the previous and our results regarding MMP2 and MMP9 roles in avian embryos, it is highly plausible that the lack in clear NCC-related phenotypes in each of the null-mice models accounts for redundant activity of one gelatinase upon its missing partner. Characterization of double MMP2–MMP9 mutants will provide an answer to this possibility.

By which precise mechanism(s) MMP9 executes NCC migration? MMP9 may promote cell migration by degrading ECM molecules and basement membrane to provide space for cell invasion, as exemplified by MMP9 activity during trophoblast invasion into the maternal decidua (Behrendtsen and Werb, 1997). Support for this activity comes from our finding where MMP9 regulated the opening of the basement membrane by cleaving laminin at sites where NCC delaminate from the neural tube. Other studies demonstrated the cleavage of another basal-membrane component, collagen IV, by MMP9 (Rodriguez et al., 2010). As collagen IV is also missing from the dorsal neural tube upon NCC migration, similar to laminin (Duband and Thiery, 1987), it is tempting to speculate that it also serves as a substrate for MMP9, especially since we show that MMP9 is localized to the same sites.

Another possible mechanism of MMP9 activity on NCC is by breaking cell–cell adhesion, enabling EMT and cell separation (Zheng et al., 2009; Zuo et al., 2011). In agreement with this possibility, we show that MMP9 is capable to rapidly degrade N-cadherin in vivo and ex-vivo. Moreover, MMP9, which is a secreted protein, is expressed in regions where N-cadherin is lost from the dorsal neural tube. However, N-cadherin is still degraded from the dorsal neural tube even when MMP9 is inhibited. This result indicates that N-cadherin serves as a substrate for MMP9 in NCC, but is also degraded by several other proteases, such as Adam 10 (Shoval et al., 2007). The orchestrated regulation and activity of these proteases should be further elucidated. Noticeably, the addition of MMP9 to neural tube explants did not diminish N-cadherin from the neural tubes, although it degraded it in the migratory NCC. This may account for reduced accessibility of MMP9 to the substrate embedded in the apical membrane of the neural tube, in contrast to the monolayer sheath of migrating NCC. Another possibility may be the production of endogenous inhibitors for MMP9 by the neural tube cells except from the dorsally-located NC progenitors. Support for this hypothesis comes from a study where TIMP2 mRNA is shown to be localized to the apical side of the neural tune apart from the most-dorsal regions (Cantemir et al., 2004). An additional attractive explanation may be that, while exogenous MMP9 is capable to degrade N-cadherin in the entire neural tube, these cells are constantly synthesizing this protein, resulting in a balance between the rate of synthesis and degradation. Indeed, some, but not full degradation is evident in the in vivo injection of MMP9 in the ventral neural tube. In contrast to neuroepithelial cells, migrating NCC are known to be prevented from expression of N-cadherin by the activity of Snail 2 (Cano et al., 2000). Thus, degradation of N-cadherin from NCC by MMP9 may not be followed by de-novo production of this adhesion molecule, resulting in its complete loss enabling the separation and EMT of the cells. Future studies will be required to assess between these different possibilities.

Finally, a different mode of action of MMP9 may be by modulating the activity of biologically-active molecules by direct cleavage, release from bound stores, or modulation of their inhibitors. For instance, MMP9 was shown to activate TGF-β by cleaving its latent associated peptide in tumor cells (Yu and Stamenkovic, 2000). Based on these examples, it is possible that, in addition to allow separation of cells and invasion into the ECM, it may modulate signals required for NCC migration. As BMP signaling is a central determinant in NCC migration (Sela-Donenfeld and Kalcheim, 1999, 2000), the feasibility of MMP9 to regulate BMP bioavailability by releasing it from bound proteins or ECM stores, or by cleaving its inhibitor, may result in promoting NCC delamination.

Supplementary materials related to this article can be found online at doi:10.1016/j.ydbio.2012.01.028.

Acknowledgments

This study was supported by The Hebrew University Fund for Innovative Research and by the bilateral fund for The University of

Hohenheim, Germany and The Hebrew University, Israel. We are grateful to Prof. Irit Sagi for providing MMP9 antibody and cDNA and Prof. Martin Blum for fruitful discussions.

References

Al Aqeel, A., Al Sewairi, W., Edress, B., Gorlin, R.J., Desnick, R.J., Martignetti, J.A., 2000. Inherited multicentric osteolysis with arthritis: a variant resembling Torg syndrome in a Saudi family. Am. J. Med. Genet. 93, 11–18.

Al-Aqeel, A.I., 2005. Al-Aqeel Sewairi syndrome, a new autosomal recessive disorder with multicentric osteolysis, nodulosis and arthropathy. The first genetic defect of matrix metalloproteinase 2 gene. Saudi Med. J. 26, 24–30.

Alfandari, D., Wolfsberg, T.G., White, J.M., DeSimone, D.W., 1997. ADAM 13: a novel ADAM expressed in somitic mesoderm and neural crest cells during *Xenopus laevis* development. Dev. Biol. 182, 314–330.

Al-Mayouf, S.M., Majeed, M., Hugosson, C., Bahabri, S., 2000. New form of idiopathic osteolysis: nodulosis, arthropathy and osteolysis (NAO) syndrome. Am. J. Med. Genet. 93, 5–10.

Anderson, R.B., 2010. Matrix metalloproteinase-2 is involved in the migration and network formation of enteric neural crest-derived cells. Int. J. Dev. Biol. 54, 63–69.

Barembaum, M., Bronner-Fraser, M., 2005. Early steps in neural crest specification. Semin. Cell Dev. Biol. 16, 642–646.

Basch, M.L., Bronner-Fraser, M., 2006. Neural crest inducing signals. Adv. Exp. Med. Biol. 589, 24–31.

Behrendtsen, O., Werb, Z., 1997. Metalloproteinases regulate parietal endoderm differentiating and migrating in cultured mouse embryos. Dev. Dyn. 208, 255–265.

Ben-Zvi, T., Yayon, A., Gertler, A., Monsonego-Ornan, E., 2006. Suppressors of cytokine signaling (SOCS) 1 and SOCS3 interact with and modulate fibroblast growth factor receptor signaling. J. Cell Sci. 119, 380–387.

Burstyn-Cohen, T., Kalcheim, C., 2002. Association between the cell cycle and neural crest delamination through specific regulation of G1/S transition. Dev. Cell 3, 383–395.

Burstyn-Cohen, T., Stanleigh, J., Sela-Donenfeld, D., Kalcheim, C., 2004. Canonical Wnt activity regulates trunk neural crest delamination linking BMP/noggin signaling with G1/S transition. Development 131, 5327–5339.

Cai, D.H., Brauer, P.R., 2002. Synthetic matrix metalloproteinase inhibitor decreases early cardiac neural crest migration in chicken embryos. Dev. Dyn. 224, 441–449.

Cai, D.H., Vollberg Sr., T.M., Hahn-Dantona, E., Quigley, J.P., Brauer, P.R., 2000. MMP-2 expression during early avian cardiac and neural crest morphogenesis. Anat. Rec. 259, 168–179.

Canete-Soler, R., Gui, Y.H., Linask, K.K., Muschel, R.J., 1995. Developmental expression of MMP-9 (gelatinase B) mRNA in mouse embryos. Dev. Dyn. 204, 30–40.

Cano, A., Perez-Moreno, M.A., Rodrigo, I., Locascio, A., Blanco, M.J., del Barrio, M.G., Portillo, F., Nieto, M.A., 2000. The transcription factor snail controls epithelial–mesenchymal transitions by repressing E-cadherin expression. Nat. Cell Biol. 2, 76–83.

Cantemir, V., Cai, D.H., Reedy, M.V., Brauer, P.R., 2004. Tissue inhibitor of metalloproteinase-2 (TIMP-2) expression during cardiac neural crest cell migration and its role in proMMP-2 activation. Dev. Dyn. 231, 709–719.

Cheung, M., Chaboissier, M.C., Mynett, A., Hirst, E., Schedl, A., Briscoe, J., 2005. The transcriptional control of trunk neural crest induction, survival, and delamination. Dev. Cell 8, 179–192.

Chin, J.R., Werb, Z., 1997. Matrix metalloproteinases regulate morphogenesis, migration and remodeling of epithelium, tongue skeletal muscle and cartilage in the mandibular arch. Development 124, 1519–1530.

Coles, E.G., Taneyhill, L.A., Bronner-Fraser, M., 2007. A critical role for Cadherin6B in regulating avian neural crest emigration. Dev. Biol. 312, 533–544.

Cousin, H., Abbruzzese, G., Kerdavid, E., Gaultier, A., Alfandari, D., 2011. Translocation of the cytoplasmic domain of ADAM13 to the nucleus is essential for Calpain8-a expression and cranial neural crest cell migration. Dev Cell 20, 256–263.

Coussens, L.M., Werb, Z., 2002. Inflammation and cancer. Nature 420, 860–867.

Coussens, L.M., Tinkle, C.L., Hanahan, D., Werb, Z., 2000. MMP-9 supplied by bone marrow-derived cells contributes to skin carcinogenesis. Cell 103, 481–490.

Dan, H., Simsa, S., Hisdai, A., Sela-Donenfeld, D., Monsonego Ornan, E., 2009. Expression of matrix metalloproteinases during impairment and recovery of the avian growth plate. J. Anim. Sci. 87, 3544–3555.

Desban, N., Lissitzky, J.C., Rousselle, P., Duband, J.L., 2006. Alpha1beta1-integrin engagement to distinct laminin-1 domains orchestrates spreading, migration and survival of neural crest cells through independent signaling pathways. J. Cell Sci. 119, 3206–3218.

Dottori, M., Gross, M.K., Labosky, P., Goulding, M., 2001. The winged-helix transcription factor Foxd3 suppresses interneuron differentiation and promotes neural crest cell fate. Development 128, 4127–4138.

Duband, J.L., Thiery, J.P., 1987. Distribution of laminin and collagens during avian neural crest development. Development 101, 461–478.

Duong, T.D., Erickson, C.A., 2004. MMP-2 plays an essential role in producing epithelial-mesenchymal transformations in the avian embryo. Dev. Dyn. 229, 42–53.

Eisen, J.S., Smith, J.C., 2008. Controlling morpholino experiments: don't stop making antisense. Development 135, 1735–1743.

Engsig, M.T., Chen, Q.J., Vu, T.H., Pedersen, A.C., Therkidsen, B., Lund, L.R., Henriksen, K., Lenhard, T., Foged, N.T., Werb, Z., et al., 2000. Matrix metalloproteinase 9 and vascular endothelial growth factor are essential for osteoclast recruitment into developing long bones. J. Cell Biol. 151, 879–889.

Erickson, C.A., 1986. Morphogenesis of the neural crest. Dev. Biol. (N Y 1985) 2, 481–543.

Erickson, C.A., 1988. Control of pathfinding by the avian trunk neural crest. Development 103 (Suppl), 63–80.

Erickson, C.A., Reedy, M.V., 1998. Neural crest development: the interplay between morphogenesis and cell differentiation. Curr. Top. Dev. Biol. 40, 177–209.

Farlie, P.G., Kerr, R., Thomas, P., Symes, T., Minichiello, J., Hearn, C.J., Newgreen, D., 1999. A paraxial exclusion zone creates patterned cranial neural crest cell outgrowth adjacent to rhombomeres 3 and 5. Dev. Biol. 213, 70–84.

Gammill, L.S., Bronner-Fraser, M., 2003. Neural crest specification: migrating into genomics. Nat. Rev. Neurosci. 4, 795–805.

Gammill, L.S., Roffers-Agarwal, J., 2010. Division of labor during trunk neural crest development. Dev. Biol. 344, 555.

Giambernardi, T.A., Sakaguchi, A.Y., Gluhak, J., Pavlin, D., Troyer, D.A., Das, G., Rodeck, U., Klebe, R.J., 2001. Neutrophil collagenase (MMP-8) is expressed during early development in neural crest cells as well as in adult melanoma cells. Matrix Biol. 20, 577–587.

Graham, A., Lumsden, A., 1996. Patterning the cranial neural crest. Biochem. Soc. Symp. 62, 77–83.

Groysman, M., Shoval, I., Kalcheim, C., 2008. A negative modulatory role for Rho and Rho-associated kinase signaling in delamination of neural crest cells. Neural Dev. 3, 27.

Hahn-Dantona, E.A., Aimes, R.T., Quigley, J.P., 2000. The isolation, characterization, and molecular cloning of a 75-kDa gelatinase B-like enzyme, a member of the matrix metalloproteinase (MMP) family. An avian enzyme that is MMP-9-like in its cell expression pattern but diverges from mammalian gelatinase B in sequence and biochemical properties. J. Biol. Chem. 275, 40827–40838.

Harrison, M., Abu-Elmagd, M., Grocott, T., Yates, C., Gavrilovic, J., Wheeler, G.N., 2004. Matrix metalloproteinase genes in *Xenopus* development. Dev. Dyn. 231, 214–220.

Hasky-Negev, M., Simsa, S., Tong, A., Genina, O., Monsonego Ornan, E., 2008. Expression of matrix metalloproteinases during vascularization and ossification of normal and impaired avian growth plate. J. Anim. Sci. 86, 1306–1315.

Holmbeck, K., Bianco, P., Caterina, J., Yamada, S., Kromer, M., Kuznetsov, S.A., Mankani, M., Robey, P.G., Poole, A.R., Pidoux, I., et al., 1999. MT1-MMP-deficient mice develop dwarfism, osteopenia, arthritis, and connective tissue disease due to inadequate collagen turnover. Cell 99, 81–92.

Itasaki, N., Bel-Vialar, S., Krumlauf, R., 1999. 'Shocking' developments in chick embryology: electroporation and in ovo gene expression. Nat. Cell Biol. 1, E203–E207.

Itoh, T., Ikeda, T., Gomi, H., Nakao, S., Suzuki, T., Itohara, S., 1997. Unaltered secretion of beta-amyloid precursor protein in gelatinase A (matrix metalloproteinase 2)-deficient mice. J. Biol. Chem. 272, 22389–22392.

Itoh, T., Tanioka, M., Matsuda, H., Nishimoto, H., Yoshioka, T., Suzuki, R., Uehira, M., 1999. Experimental metastasis is suppressed in MMP-9-deficient mice. Clin. Exp. Metastasis 17, 177–181.

Jhingory, S., Wu, C.Y., Taneyhill, L.A., 2010. Novel insight into the function and regulation of [alpha]N-catenin by Snail2 during chick neural crest cell migration. Developmental Biology 344, 896.

Kalcheim, C., 2000. Mechanisms of early neural crest development: from cell specification to migration. Int. Rev. Cytol. 200, 143–196.

Kalcheim, C., Burstyn-Cohen, T., 2005. Early stages of neural crest ontogeny: formation and regulation of cell delamination. Int. J. Dev. Biol. 49, 105–116.

Kinoh, H., Sato, H., Tsunezuka, Y., Takino, T., Kawashima, A., Okada, Y., Seiki, M., 1996. MT-MMP, the cell surface activator of proMMP-2 (pro-gelatinase A), is expressed with its substrate in mouse tissue during embryogenesis. J. Cell Sci. 109 (Pt 5), 953–959.

Kulesa, P.M., Gammill, L.S., 2010. Neural crest migration: patterns, phases and signals. Dev. Biol. 344, 566.

Leach Jr., R.M., Monsonego-Ornan, E., 2007. Tibial dyschondroplasia 40 years later. Poult. Sci. 86, 2053–2058.

Le-Douarin, N.M., Kalcheim, C., 1999. The Neural Crest, 2nd edn. Cambridge University Press.

Lelongt, B., Trugnan, G., Murphy, G., Ronco, P.M., 1997. Matrix metalloproteinases MMP2 and MMP9 are produced in early stages of kidney morphogenesis but only MMP9 is required for renal organogenesis in vitro. J. Cell Biol. 136, 1363–1373.

Levin, J.I., Chen, J., Du, M., Hogan, M., Kincaid, S., Nelson, F.C., Venkatesan, A.M., Wehr, T., Zask, A., DiJoseph, J., et al., 2001. The discovery of anthranilic acid–based MMP inhibitors. Part 2: SAR of the 5-position and P1(1) groups. Bioorg. Med. Chem. Lett. 11, 2189–2192.

Lohi, J., Wilson, C.L., Roby, J.D., Parks, W.C., 2001. Epilysin, a novel human matrix metalloproteinase (MMP-28) expressed in testis and keratinocytes and in response to injury. J. Biol. Chem. 276, 10134–10144.

Malemud, C.J., 2006a. Matrix metalloproteinases (MMPs) in health and disease: an overview. Front. Biosci. 11, 1696–1701.

Malemud, C.J., 2006b. Matrix metalloproteinases: role in skeletal development and growth plate disorders. Front. Biosci. 11, 1702–1715.

Martignetti, J.A., Aqeel, A.A., Sewairi, W.A., Boumah, C.E., Kambouris, M., Mayouf, S.A., Sheth, K.V., Eid, W.A., Dowling, O., Harris, J., et al., 2001. Mutation of the matrix metalloproteinase 2 gene (MMP2) causes a multicentric osteolysis and arthritis syndrome. Nat. Genet. 28, 261–265.

Martinez-Morales, P.L., Diez del Corral, R., Olivera-Martinez, I., Quiroga, A.C., Das, R.M., Barbas, J.A., Storey, K.G., Morales, A.V., 2011. FGF and retinoic acid activity gradients control the timing of neural crest cell emigration in the trunk. J. Cell Biol. 194, 489–503.

McCawley, L.J., Matrisian, L.M., 2000. Matrix metalloproteinases: multifunctional contributors to tumor progression. Mol. Med. Today 6, 149–156.

Miettinen, P.J., Chin, J.R., Shum, L., Slavkin, H.C., Shuler, C.F., Derynck, R., Werb, Z., 1999. Epidermal growth factor receptor function is necessary for normal craniofacial development and palate closure. Nat. Genet. 22, 69–73.

Monsonego-Ornan, E., Adar, R., Feferman, T., Segev, O., Yayon, A., 2000. The transmembrane mutation G380R in fibroblast growth factor receptor 3 uncouples ligand-mediated receptor activation from down-regulation. Mol. Cell. Biol. 20, 516–522.
Morrison, C.J., Butler, G.S., Rodriguez, D., Overall, C.M., 2009. Matrix metalloproteinase proteomics: substrates, targets, and therapy. Curr. Opin. Cell Biol. 21, 645–653.
Mosig, R.A., Dowling, O., DiFeo, A., Ramirez, M.C., Parker, I.C., Abe, E., Diouri, J., Aqeel, A.A., Wylie, J.D., Oblander, S.A., et al., 2007. Loss of MMP-2 disrupts skeletal and craniofacial development and results in decreased bone mineralization, joint erosion and defects in osteoblast and osteoclast growth. Hum. Mol. Genet. 16, 1113–1123.
Mott, J.D., Werb, Z., 2004. Regulation of matrix biology by matrix metalloproteinases. Curr. Opin. Cell Biol. 16, 558–564.
Nagase, H., Woessner Jr., J.F., 1999. Matrix metalloproteinases. J. Biol. Chem. 274, 21491–21494.
Nakagawa, S., Takeichi, M., 1995. Neural crest cell–cell adhesion controlled by sequential and subpopulation-specific expression of novel cadherins. Development 121, 1321–1332.
Nakagawa, S., Takeichi, M., 1998. Neural crest emigration from the neural tube depends on regulated cadherin expression. Development 125, 2963–2971.
Nelson, A.R., Fingleton, B., Rothenberg, M.L., Matrisian, L.M., 2000. Matrix metalloproteinases: biologic activity and clinical implications. J. Clin. Oncol. 18, 1135–1149.
Newgreen, D.F., Minichiello, J., 1995. Control of epitheliomesenchymal transformation. I. Events in the onset of neural crest cell migration are separable and inducible by protein kinase inhibitors. Dev. Biol. 170, 91–101.
Nieto, M.A., Bradley, L.C., Wilkinson, D.G., 1991. Conserved segmental expression of Krox-20 in the vertebrate hindbrain and its relationship to lineage restriction. Development (Suppl. 2), 59–62.
Perez, S.E., Cano, D.A., Dao-Pick, T., Rougier, J.P., Werb, Z., Hebrok, M., 2005. Matrix metalloproteinases 2 and 9 are dispensable for pancreatic islet formation and function in vivo. Diabetes 54, 694–701.
Perris, R., Paulsson, M., Bronner-Fraser, M., 1989. Molecular mechanisms of avian neural crest cell migration on fibronectin and laminin. Dev. Biol. 136, 222.
Radisky, D.C., 2005. Epithelial–mesenchymal transition. J. Cell Sci. 118, 4325–4326.
Raible, D.W., 2006. Development of the neural crest: achieving specificity in regulatory pathways. Curr. Opin. Cell Biol. 18, 698–703.
Randall, L.E., Hall, R.C., 2002. Temperospatial expression of matrix metalloproteinases 1, 2, 3, and 9 during early tooth development. Connect. Tissue Res. 43, 205–211.
Reich, A., Jaffe, N., Tong, A., Lavelin, I., Genina, O., Pines, M., Sklan, D., Nussinovitch, A., Monsonego-Ornan, E., 2005. Weight loading young chicks inhibits bone elongation and promotes growth plate ossification and vascularization. J. Appl. Physiol. 98, 2381–2389.
Reponen, P., Sahlberg, C., Huhtala, P., Hurskainen, T., Thesleff, I., Tryggvason, K., 1992. Molecular cloning of murine 72-kDa type IV collagenase and its expression during mouse development. J. Biol. Chem. 267, 7856–7862.
Rodriguez, D., Morrison, C.J., Overall, C.M., 2010. Matrix metalloproteinases: what do they not do? New substrates and biological roles identified by murine models and proteomics. Biochim Biophys Acta 1803, 39–54.
Sela-Donenfeld, D., Kalcheim, C., 1999. Regulation of the onset of neural crest migration by coordinated activity of BMP4 and Noggin in the dorsal neural tube. Development 126, 4749–4762.
Sela-Donenfeld, D., Kalcheim, C., 2000. Inhibition of noggin expression in the dorsal neural tube by somitogenesis: a mechanism for coordinating the timing of neural crest emigration. Development 127, 4845–4854.
Sela-Donenfeld, D., Kalcheim, C., 2002. Localized BMP4-noggin interactions generate the dynamic patterning of noggin expression in somites. Dev. Biol. 246, 311–328.
Sela-Donenfeld, D., Kayam, G., Wilkinson, D., 2009. Boundary cells regulate a switch in the expression of FGF3 in hindbrain rhombomeres. BMC Dev. Biol. 9, 16.
Shelton, E.L., Yutzey, K.E., 2007. Tbx20 regulation of endocardial cushion cell proliferation and extracellular matrix gene expression. Dev. Biol. 302, 376–388.
Shimo, T., Kanyama, M., Wu, C., Sugito, H., Billings, P.C., Abrams, W.R., Rosenbloom, J., Iwamoto, M., Pacifici, M., Koyama, E., 2004. Expression and roles of connective tissue growth factor in Meckel's cartilage development. Dev. Dyn. 231, 136–147.
Shoval, I., Ludwig, A., Kalcheim, C., 2007. Antagonistic roles of full-length N-cadherin and its soluble BMP cleavage product in neural crest delamination. Development 134, 491–501.
Simsa, S., Genina, O., Ornan, E.M., 2007a. Matrix metalloproteinase expression and localization in turkey (*Meleagris gallopavo*) during the endochondral ossification process. J. Anim. Sci. 85, 1393–1401.
Simsa, S., Hasdai, A., Dan, H., Ornan, E.M., 2007b. Differential regulation of MMPs and matrix assembly in chicken and turkey growth-plate chondrocytes. Am. J. Physiol. Regul. Integr. Comp. Physiol. 292, R2216–R2224.
Sternlicht, M.D., Werb, Z., 2001. How matrix metalloproteinases regulate cell behavior. Annu. Rev. Cell Dev. Biol. 17, 463–516.
Taneyhill, L.A., 2008. To adhere or not to adhere: the role of cadherins in neural crest development. Cell Adh. Migr. 2, 223–230.
Taylor, K.M., LaBonne, C., 2007. Modulating the activity of neural crest regulatory factors. Curr. Opin. Genet. Dev. 17, 326–331.
Thiery, J.P., Boyer, B., Tucker, G., Gavrilovic, J., Valles, A.M., 1988. Adhesion mechanisms in embryogenesis and in cancer invasion and metastasis. CIBA Found. Symp. 141, 48–74.
Tomlinson, M.L., Garcia-Morales, C., Abu-Elmagd, M., Wheeler, G.N., 2008. Three matrix metalloproteinases are required in vivo for macrophage migration during embryonic development. Mech Dev.
Tomlinson, M.L., Guan, P., Morris, R.J., Fidock, M.D., Rejzek, M., Garcia-Morales, C., Field, R.A., Wheeler, G.N., 2009. A chemical genomic approach identifies matrix metalloproteinases as playing an essential and specific role in *Xenopus* melanophore migration. Chem. Biol. 16, 93–104.
Tong, A., Reich, A., Genin, O., Pines, M., Monsonego-Ornan, E., 2003. Expression of chicken 75-kDa gelatinase B-like enzyme in perivascular chondrocytes suggests its role in vascularization of the growth plate. J. Bone Miner. Res. 18, 1443–1452.
Trainor, P.A., 2005. Specification of neural crest cell formation and migration in mouse embryos. Semin. Cell Dev. Biol. 16, 683–693.
Tzu, J., Marinkovich, M.P., 2008. Bridging structure with function: structural, regulatory, and developmental role of laminins. Int. J. Biochem. Cell Biol. 40, 199–214.
Visse, R., Nagase, H., 2003. Matrix metalloproteinases and tissue inhibitors of metalloproteinases: structure, function, and biochemistry. Circ. Res. 92, 827–839.
Vu, T.H., Werb, Z., 2000. Matrix metalloproteinases: effectors of development and normal physiology. Genes Dev. 14, 2123–2133.
Vu, T.H., Shipley, J.M., Bergers, G., Berger, J.E., Helms, J.A., Hanahan, D., Shapiro, S.D., Senior, R.M., Werb, Z., 1998. MMP-9/gelatinase B is a key regulator of growth plate angiogenesis and apoptosis of hypertrophic chondrocytes. Cell 93, 411–422.
Wei, S., Xu, G., Bridges, L.C., Williams, P., White, J.M., DeSimone, D.W., 2010. ADAM13 induces cranial neural crest by cleaving class B ephrins and regulating Wnt signaling. Developmental Cell 19, 345.
Weisinger, K., Wilkinson, G.D., Sela-Donenfeld, D., 2008. Inhibition of BMPs by follistatin is required for FGF3 expression and segmental patterning of the hindbrain. Developmental Biology.
Weizmann, S., Tong, A., Reich, A., Genina, O., Yayon, A., Monsonego-Ornan, E., 2005. FGF upregulates osteopontin in epiphyseal growth plate chondrocytes: implications for endochondral ossification. Matrix Biol 24, 520–529.
Wright, J., Cooley, B., Duwell, J., Sieber-Blum, M., 1988. Migration-related changes in the cytoskeleton of cultured neural crest cells visualized by the monoclonal antibody I-5G9. J. Neurosci. Res. 21, 148–154.
Yu, Q., Stamenkovic, I., 2000. Cell surface-localized matrix metalloproteinase-9 proteolytically activates TGF-beta and promotes tumor invasion and angiogenesis. Genes Dev. 14, 163–176.
Zheng, G., Lyons, J.G., Tan, T.K., Wang, Y., Hsu, T.-T., Min, D., Succar, L., Rangan, G.K., Hu, M., Henderson, B.R., et al., 2009. Disruption of E-cadherin by matrix metalloproteinase directly mediates epithelial–mesenchymal transition downstream of transforming growth factor-β1 in renal tubular epithelial cells. Am. J. Pathol. 175, 580–591.
Zhou, Z., Apte, S.S., Soininen, R., Cao, R., Baaklini, G.Y., Rauser, R.W., Wang, J., Cao, Y., Tryggvason, K., 2000. Impaired endochondral ossification and angiogenesis in mice deficient in membrane-type matrix metalloproteinase I. Proc. Natl. Acad. Sci. U. S. A. 97, 4052–4057.
Zuo, J.-H., Zhu, W., Li, M.-Y., Li, X.-H., Yi, H., Zeng, G.-Q., Wan, X.-X., He, Q.-Y., Li, J.-H., Qu, J.-Q., et al., 2011. Activation of EGFR promotes squamous carcinoma SCC10A cell migration and invasion via inducing EMT-like phenotype change and MMP-9-mediated degradation of E-cadherin. J. Cell. Biochem. 112, 2508–2517.